AN EXPERIMENTAL AND THEORETICAL COMPARISON
OF ROTORDYNAMIC COEFFICIENTS FOR
SAWTOOTH-PATTERN DAMPER SEALS

A Thesis By

Steven Anthony Nolan

SEAL-1-87

NASA-CR-179026

(NASA-CR-179026) AN EXPERIMENTAL AND THEORETICAL COMPARISON OF ROTORDYNAMIC COEFFICIENTS FOR SAWTOOTH-PATTERN DAMPER SEALS M.S. Thesis (Texas A&M Univ.) 83 p CSCL 11A G3/37 N87-18819 Unclas 43623

Turbomachinery Laboratories
Mechanical Engineering Department

AN EXPERIMENTAL AND THEORETICAL COMPARISON OF ROTORDYNAMIC COEFFICIENTS FOR SAWTOOTH-PATTERN DAMPER SEALS

A Thesis

by

STEVEN ANTHONY NOLAN

Submitted to the Graduate College of
Texas A&M University
in partial fulfillment of the requirements for the degree of

MASTER OF SCIENCE

May 1987

Major Subject: Mechanical Engineering

ABSTRACT

An Experimental and Theoretical Comparison
of Rotordynamic Coefficients for
Sawtooth-pattern Damper Seals (May 1987)
Steven Anthony Nolan, B.S., Texas A&M University
Chairman of Advisory Committee: Dr. Dara Childs

This report presents a brief review of annular seal theory as related to rotordynamics for liquid seals . It also includes an overview of Childs and Kim's [11] current theory for calculating empirical turbulence coefficients and predicting stiffness and damping coefficients for surface roughened "damper" seals. The designation "sawtooth-pattern" refers to a seal stator with a roughness pattern whose cross section normal to the seal axis resembles a sawtooth with the teeth directed against the flow. The net stiffness and damping coefficients for the eleven seals are compared to each other, a smooth seal, and the optimum-configuration damper seal previously tested. The experimental force coefficients, the net damping, and the net stiffness coefficients for four of the sawtooth seals are compared to the predictions of Childs and Kim's analysis.

The sawtooth pattern seals had less net damping than the hole-pattern seal but more than the smooth seal. The stiffness was comparable to the hole-pattern seal. Both the sawtooth and hole-pattern seals leaked less than the smooth seal, while the sawtooth-pattern seal with maximum damping leaked more than the hole-pattern seal. The

PRECEDING PAGE BLANK NOT FILMED

theoretical predictions compared relatively poorly to the experimental results obtained for the rotordynamic coefficients of the seals investigated.

ACKNOWLEDGEMENT

The author wishes to express his sincere appreciation to Dr. D. W. Childs for his help and guidance throughout this project. The author also thanks Mr. Keith Hale, Mr. Dean Nunez and Ms. Vondell Scharrer for their additional assistance. This project has been principally supported by NASA Contract NAS8-35824 from the George C. Marshall Space Flight Center.

TABLE OF CONTENTS

		Page
	ABSTRACT	iii
	ACKNOWLEDGEMENT	v
	TABLE OF CONTENTS	vi
	LIST OF TABLES	vii
	LIST OF FIGURES	viii
	NOMENCLATURE	xi
CHAPTER		
I	INTRODUCTION	1
II	TEST APPARATUS AND METHOD	8
	Apparatus	8
	Stator configurations	10
	Dynamic test data	12
III	TEST RESULTS: RELATIVE PERFORMANCE OF SEALS	19
	Stators 1 through 4	19
	Stators 5 through 7	23
	Stators 8 through 11	27
	Best relative performance	27
IV	ANALYSIS	32
	Empirical turbulence coefficients	35
V	THEORY VERSUS EXPERIMENT : FORCE COEFFICIENTS	51
	Introduction	51
	Dynamic data	51
	Rotordynamic coefficient Comparison	52
VI	CONCLUSIONS	58
	REFERENCES	60
	APPENDIX A	62
	VITA	71

LIST OF TABLES

Table		Page
1	Dimensions of sawtooth-pattern stators.	11
2	Empirical coefficients for stators 8-11	45
3	Experimental and theoretical comparison of K_{ef} for stators 8 through 11.	53
4	Experimental and theoretical comparison of C_{ef} for stators 8 through 11.	54
5	Experimental and theoretical comparison of M_{ef} for stators 8 through 11.	55
6	Comparison of theoretical and measured values for stiffness, damping, and added-mass coefficients	57

LIST OF FIGURES

Figure		Page
1	Interstage and neck-ring seals for a centrifugal pump	2
2	Round-hole-pattern damper seal	5
3	Sawtooth-pattern damper seal cross section	6
4	High Reynolds number test section	9
5	Schematic for sawtooth pattern stators 1 through 4	13
6	Schematic for sawtooth pattern stators 5 through 7	14
7	Schematic for sawtooth pattern stators 8 through 11	15
8	C_{ef} for sawtooth stators 1 through 4, optimum hole-pattern damper seal and a smooth seal	20
9	K_{ef} for sawtooth stators 1 through 4, optimum hole-pattern damper seal and a smooth seal	21
10	$C_d^{-1/2}$ for sawtooth stators 1 through 4, optimum hole-pattern damper seal and a smooth seal	22
11	C_{ef} for sawtooth stators 5 through 7, optimum hole-pattern damper seal and a smooth seal	24
12	K_{ef} for sawtooth stators 5 through 7, optimum hole-pattern damper seal and a smooth seal	25
13	$C_d^{-1/2}$ for sawtooth stators 5 through 7, optimum hole-pattern damper seal and a smooth seal	26
14	C_{ef} for sawtooth stators 8 through 11, optimum hole-pattern damper seal and a smooth seal	28

Figure Page

15 K_{ef} for sawtooth stators 8 through 11, optimum hole-pattern damper seal and a smooth seal. 29

16 $C_d^{-1/2}$ for sawtooth stators 8 through 11, optimum hole-pattern damper seal and a smooth seal. 30

17 Differential Fluid Element 33

18 Flowchart for the solution of the empirical coefficients for equal rotor and stator surface roughnesses. 41

19 Experimental and calculated values for σ based on calculated empirical coefficients for a smooth seal 42

20 Flowchart for the solution of stator empirical turbulence coefficients m_s, n_s from test data and known rotor coefficients 44

21 Experimental and calculated values for σ for stator #8. 46

22 Experimental and calculated values for σ for stator #9. 47

23 Experimental and calculated values for σ for stator #10 48

24 Experimental and calculated values for σ for stator #11 49

A1 Experimental and theoretical results for radial force coefficients for stator 8. 63

Figure Page

A2 Experimental and theoretical results for tangential force coefficients for stator 8 64

A3 Experimental and theoretical results for radial force coefficients for stator 9 65

A4 Experimental and theoretical results for tangential force coefficients for stator 9 66

A5 Experimental and theoretical results for radial force coefficients for stator 10. 67

A6 Experimental and theoretical results for tangential force coefficients for stator 10. 68

A7 Experimental and theoretical results for radial force coefficients for stator 11. 69

A8 Experimental and theoretical results for tangential force coefficients for stator 11. 70

NOMENCLATURE

A = Dynamic seal eccentricity (L)

C, c = Direct and cross-coupled damping coefficients (FL/T)

K, k = Direct and cross-coupled stiffness coefficients (F/L)

C_{ef} = Net damping coefficient (FL/T)

K_{ef} = Net stiffness coefficient (F/L)

C_d = Discharge coefficient

C_r = Minimum seal radial clearence (L)

F_x, F_y = Cartesian components of the seal reaction force (F)

F_r, F_θ = Radial and tangential components of the reaction force (F)

$H(\theta, t)$ = Seal clearence function (L)

M = Seal added mass coefficient (M)

M_{ef} = Effective seal added mass coefficient (M)

m_r, n_r = Empirical turbulence coefficients to define rotor friction factor

m_s, n_s = Empirical turbulence coefficients to define stator friction factor

P = Fluid pressure in the seal (F/L^2)

ΔP = Pressure drop across the seal. (F/L^2)

R = Seal radius (L)

R_a = $2\rho VH/\mu$ = Reynolds-number

U_θ = Circumferential fluid velocity (L/T)

U_z = Axial fluid velocity (L/T)

u_θ = $U_\theta/R\omega$ = nondimensional circumferential fluid velocity

u_z = U_z/V = nondimensional axial fluid velocity

V = Average axial fluid velocity in the seal (L/T)

X, Y = Seal displacement components (L)

λ_r = Rotor friction factor

λ_s = Stator friction factor

σ = $\lambda(L/C_r)$= Axial pressure gradient coefficient

ρ = Fluid density (M/L^3)

ω = Seal rotational and precessional velocity (T^{-1})

μ = Fluid viscosity (FT/L^2)

Subscripts

r rotor

s stator

z axial

θ circumferential

0 zeroth-order equation variable

1 first-order equation variable

CHAPTER I

INTRODUCTION

Experience has shown that liquid pump seals can have a significant effect on pump rotordynamic characteristics. In a series of publications Black and Jenssen [1,2,3,4] explained the influence of seal forces on pump rotordynamic behavior. Additionally, stability problems with the Space Shuttle Main Engine were found to be crucially dependent on its interstage seal design [5], prompting further research into the forces developed by liquid seals.

The two types of pump seals which have potential for developing significant rotor forces are illustrated in Fig. 1. The neck- or wear-ring seals reduce the back leakage flow along the front surface of the impeller. The interstage seals reduce the leakage from an impeller inlet back along the shaft to the back side of the preceding impeller. Both of these seals can significantly influence the rotordynamic response of any multistage pump.

As related to rotordynamics, analysis of seals has the objective of defining reaction forces acting on the rotor as a consequence of shaft motion. Due to the similarities between annular seals and journal bearings, seal analysis is generally based on governing equations developed for bearings.

A linearized seal model which applies for small motion of the rotor about a centered position in the seal and relates reaction forces

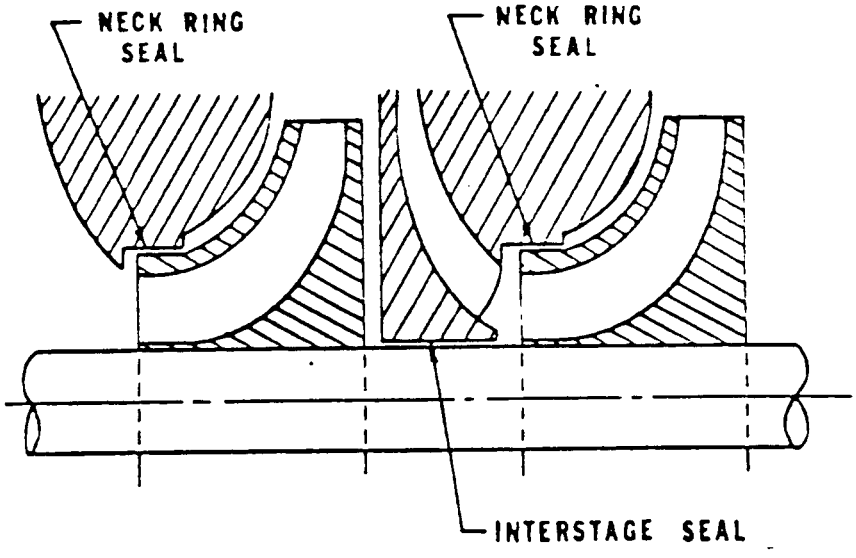

Fig. 1 Interstage and neck-ring seals for a centrifugal pump

and shaft motion is expressed:

$$-\begin{Bmatrix} F_x \\ F_y \end{Bmatrix} = \begin{bmatrix} K & k \\ -k & K \end{bmatrix} \begin{Bmatrix} X \\ Y \end{Bmatrix} + \begin{bmatrix} C & c \\ -c & C \end{bmatrix} \begin{Bmatrix} \dot{X} \\ \dot{Y} \end{Bmatrix} + M \begin{Bmatrix} \ddot{X} \\ \ddot{Y} \end{Bmatrix} \qquad (1)$$

In Eq. 1 the diagonal coefficients are referred to as "direct", while the off diagonal coefficients are referred to as "cross-coupled" due to the coupling effect they exhibit. That is, motion in one plane causes a reaction force in an orthogonal one.

While annular seals and journal bearings may be geometrically similar, they differ in that seals typically have radial clearence-to-radius ratios on the order of 0.005 as apposed to 0.001 for bearings. Because of these clearences and the pressure differential across the seal, fully-developed turbulent flow usually exists in the seal. Additionally, unlike plain journal bearings, seals develop a significant direct stiffness in the centered position. This phenomenon, first pointed out by Lomakin [6], arises due to the distribution of the pressure drop between (a) inlet losses, and (b) the axial pressure gradient caused by wall friction losses.

Early analytical and experimental developments generally dealt with the "smooth" seal where both the rotor and stator were assumed to have the same nominally smooth surface roughness. These early analytical and experimental developments are provided in Childs' [7,8] finite-length solution analysis. Childs' finite-length analysis of constant-clearance and convergent-tapered turbulent seals for small motion about a centered position was based on Hirs' [9] turbulent

lubrication equation. The analysis and solutions presented in [7] and [8] incorporated all of Black et al.'s [2,3,4] various developments and used a single derivation from one set of governing equations yielding results which included all previous developments.

To improve the rotordynamic characteristics of pump seals, the "damper seal" which employs a smooth rotor and deliberately surface-roughened stator was proposed by von Pragenau [10]. Von Pragenau's analysis demonstrated that the damper seal yields lower asymptotic circumferential fluid velocities in the seal which implies a reduction of the cross-coupled stiffness. Since the cross-coupled stiffness produced a destabilizing force, the reduction in cross-coupled stiffness increased the rotordynamic stability.

The damper seal was further studied by Childs and Kim [11]. They developed a finite-length numerical solution for the damper seal based on a slight modification to Hirs' governing equations to account for different surface roughnesses on the rotor and stator elements. Childs and Kim also reported encouraging analytical and experimental results for several hole-pattern damper seals [12], which had a configuration as illustrated in Fig.2.

Encouraging experimental results [13] for the original sawtooth-pattern axial groove seal led to the proposal of testing and analysis of a sawtooth pattern damper seal. The sawtooth-pattern seal is based on the idea that directing the teeth of the sawtooth-pattern cross section against the fluid rotation, as shown in Fig. 3, will further reduce the asymptotic circumferential fluid velocities and hence, increase the rotordynamic stability.

ORIGINAL PAGE IS
OF POOR QUALITY

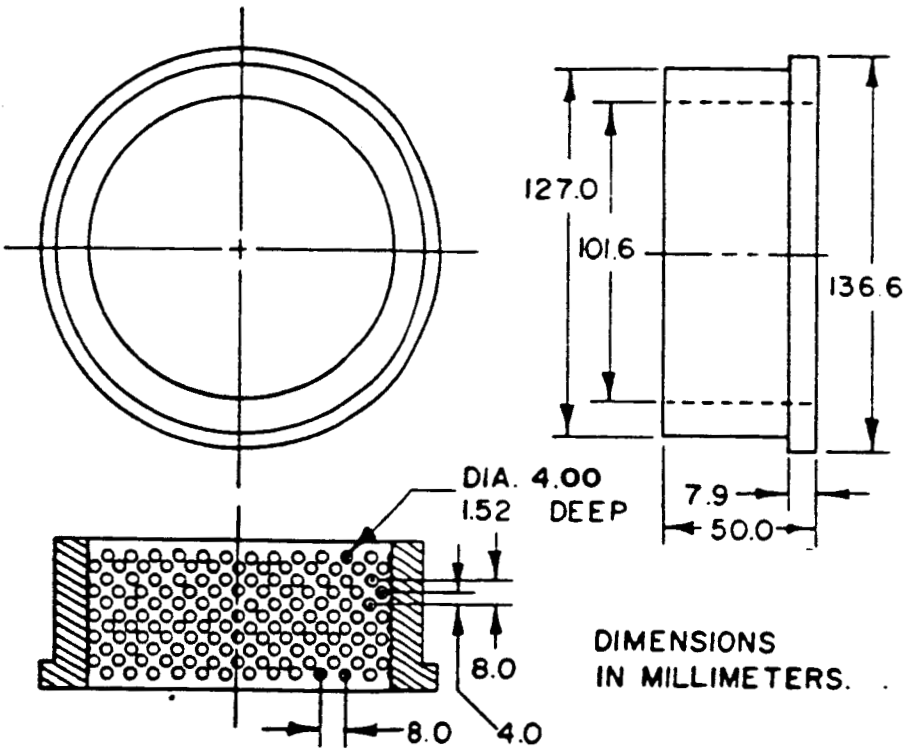

Fig. 2 Round-hole-pattern damper seal

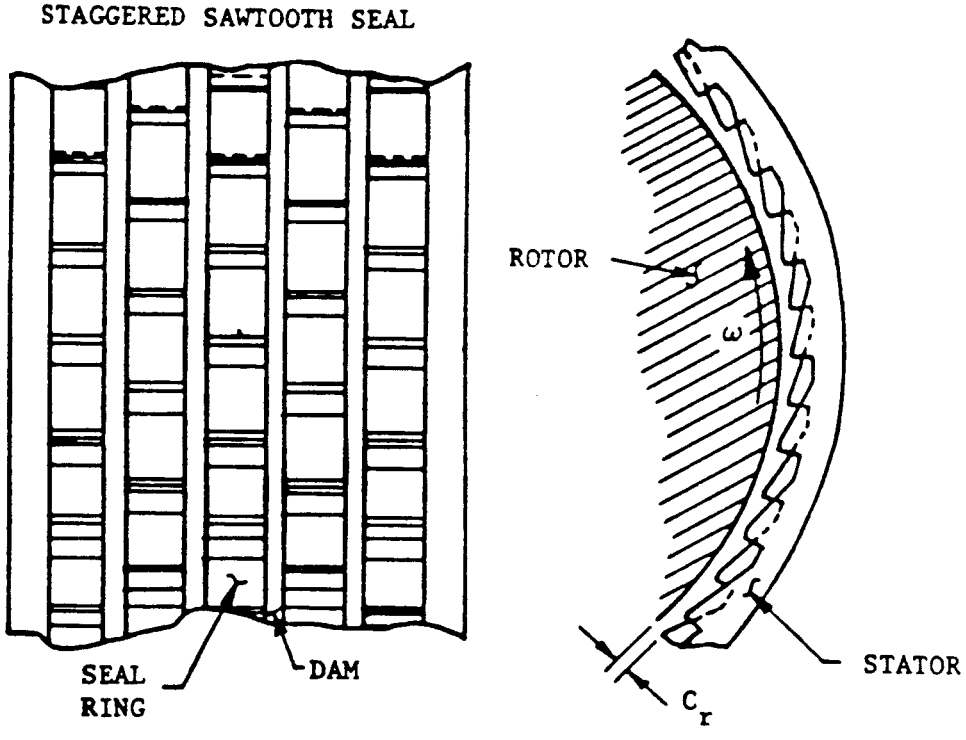

Fig. 3 Sawtooth-pattern damper seal cross section

Due to the importance of rotordynamic response, this report examines the effects of geometric variations in the sawtooth pattern seals on the rotordynamic coefficients. Based on the results from the sawtooth, axial-groove seal [13], the idea was examined that a sawtooth pattern seal could be developed with better rotordynamic characteristics than the hole-pattern damper seal.

Childs and Kim's analysis is the most complete current analysis for calculating dynamic coefficients of surface roughened seals and was used to obtain a theoretical comparison for the experimental data for several of the sawtooth-pattern seals. Although the sawtooth pattern seals do not entirely conform to Childs and Kim's requirement of having a directionally homogeneous surface roughness, several of the seals had an approximately homogeneous surface roughness. The seals which are compared to theory are those with "square" holes which provided a somewhat homogeneous surface roughness on the seal surface.

CHAPTER II

TEST APPARATUS AND METHOD

The experimental results reported here were developed as part of an extended, NASA-funded, high Reynolds-number test program of pump seal configurations in support of the SSME (Space Shuttle Main Engine) development program. Most of the detailed information discussing the test facility description, the data aquisition, and the testing procedures is not repeated here, but is available in earlier reports [13,14]. This section reviews the test section and seal configurations and the method used to obtain the stiffness and damping coefficients for the seals.

Apparatus. High Reynolds-numbers, comparable to those occuring in the SSME cryogenic turbopumps, are achieved using Halon, $CBrF_3$, as a test fluid. Halon is a Dupont-manufactured fire-extinguisher fluid and refrigerant which combines a low absolute viscosity and high density resulting in a kinematic viscosity, actually lower than liquid hydrogen [15]. The seal test section is shown in Fig. 4. Fluid enters the test section in the center and is discharged axially through the test seals, which are stator inserts pressed into the test section housing. The seal rotor segments are mounted eccentrically on the rotor shaft with a given eccentricity A. Rotation of the eccentrically mounted segments produces a synchronously-precessing pressure field. The transient pressure field is measured by axially-spaced, strain-gauge pressure transducers. The relative rotor motion X(t), Y(t) is simultaneously

ORIGINAL PAGE IS
OF POOR QUALITY

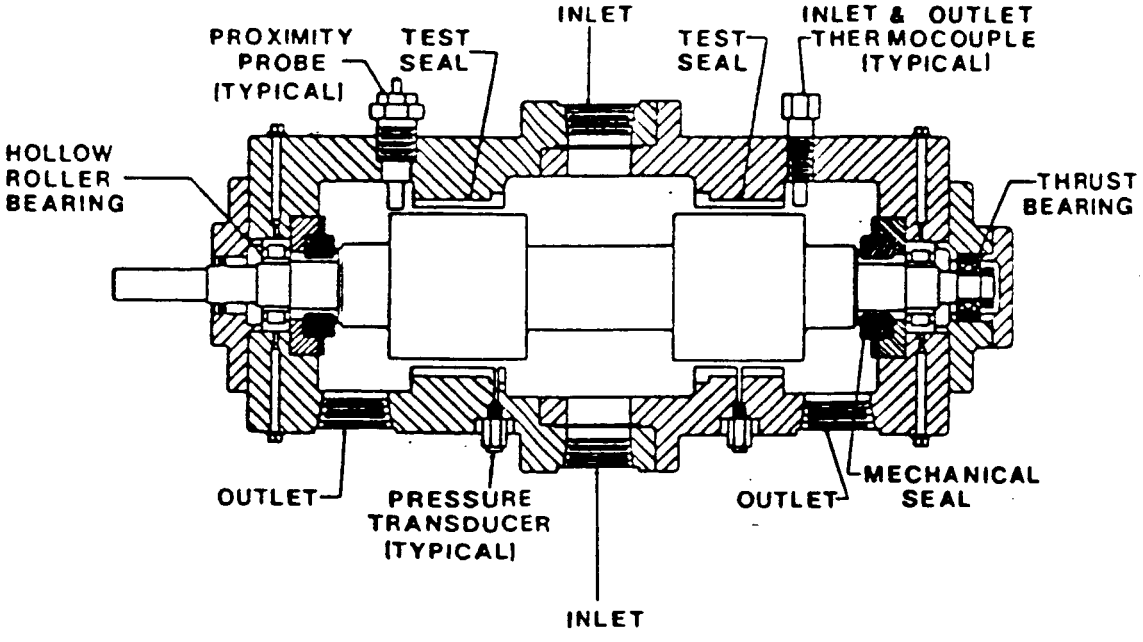

Fig. 4 High Reynolds-number test section

measured by capacitance-type proximity probes. The transient pressure field measurements are integrated and resolved parallel and normal to the rotor eccentricity vector to define F_r/A and F_θ/A respectively. For a given test, five to ten cycles of data, containing on the order of 2000 data points, are recorded and analyzed to yield a calculated average and standard deviation for F_r/A and F_θ/A.

Stator configurations. All of the sawtooth-pattern seals tested have the same 4 inch (101.6 mm) internal diameter, 1.96 inch (49.9 mm) length, and 0.020 inch (.508 mm) minimum radial clearance. The seal geometries are varied by changing the tooth groove depth, width, and length as well as the number of teeth and the number of spacer elements or "dams." Important dimensions for all eleven seals are provided in Table 1.

In the testing of hole-pattern damper seals, [12] the parameter

$$\gamma = \frac{\text{hole area}}{\text{total surface area}}$$

was found to be useful in predicting seal performance. For the sawtooth-pattern seals the hole is defined as the portion of the groove between the dams; thus, a single hole has the area $A_h = B \cdot E$. The ratio of the groove depth to minimum radial clearance, h/C_r, is also included in Table 1. The seals are grouped where stators 1 through 4 have an h/C_r ratio of 4.8, while stators 5 through 7, and 8 through 11 have h/C_r ratios of 1.9 and 2.9, respectively.

The dimensions and arrangements of stators 1 through 4 are

ORIGINAL PAGE IS
OF POOR QUALITY

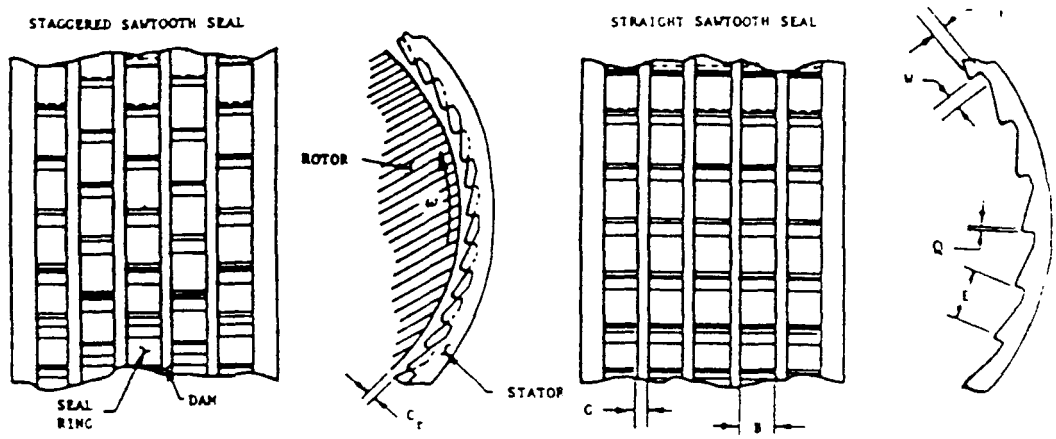

SEAL	TEETH	SEAL RINGS	DAMS	TYPE	h (mm)	W (mm)	Q (mm)	E (mm)	G (mm)	B (mm)	Y	h/C_r
1	25	5	4	straight	2.54	3.81	0.508	12.36	4.92	4.15	.40	4.8
2	25	5	4	staggered	2.54	3.81	0.508	12.36	4.92	4.15	.40	4.8
3	25	5	4	straight	2.54	3.81	0.508	12.36	0.48	7.70	.74	4.8
4	25	5	4	staggered	2.54	3.81	0.508	12.36	0.48	7.70	.74	4.8
5	105	5	4	straight	1.02	0.0	0.508	2.54	0.48	7.70	.64	1.9
6	80	5	4	straight	1.02	0.0	1.448	2.54	0.48	7.70	.49	1.9
7	55	5	4	straight	1.02	0.0	3.251	2.54	0.48	7.70	.34	1.9
8	60	8	7	staggered	1.52	2.42	0.478	4.84	1.98	3.32	.48	2.9
9	60	8	7	staggered	1.52	2.42	0.477	4.84	0.48	4.64	.68	2.9
10	60	8	7	staggered	1.52	1.67	1.985	3.34	1.98	3.32	.33	2.9
11	60	8	7	staggered	1.52	1.67	1.984	3.34	0.48	4.63	.47	2.9

Table 1. Dimensions of sawtooth-pattern stators

illustrated in Fig 5. The groove depth for these seals is 0.10 inches (2.54 mm), which is quite large for damper seals. The sawtooth alignment is varied for these four seals with the grooves of seals 1 and 3 being aligned (straight configuration), and seals 2 and 4 have the grooves staggered.

The dimensions and configurations for stators 5 through 7 are illustrated in Fig. 6. These three seals have a tooth depth of 0.04 inches (1.02 mm.) and also have a straight groove configuration. The stator cross sections only differ in the number of teeth in each.

The configurations and dimensions for stators 8 through 11 are illustrated in Fig. 7. These stators all have a staggered tooth configuration. The groove depth for these four seals is 0.060 inches (1.52 mm).

Dynamic test data. For each seal configuration the data are gathered from a test matrix which is obtained by varying the running speed and flow rate, and hence the axial Reynolds-number. The flow rate range varies between the maximum capacity of the supply pump and the minimum flow corresponding to a ΔP sufficient to generate reasonable transient pressure signals in the test section. For any given Reynolds-number, the rotor speed is varied over the running speed capacities of the drive motors from approximately 1000 RPM to 7200 RPM. The resulting data are in the form of radial and tangential force coefficients F_r/A and F_θ/A as determined by integrating the transient pressure field . These force coefficients are presented as functions of the running speed for a given axial Reynolds number value.

To compare the relative performance of the different seal

ORIGINAL PAGE IS
OF POOR QUALITY

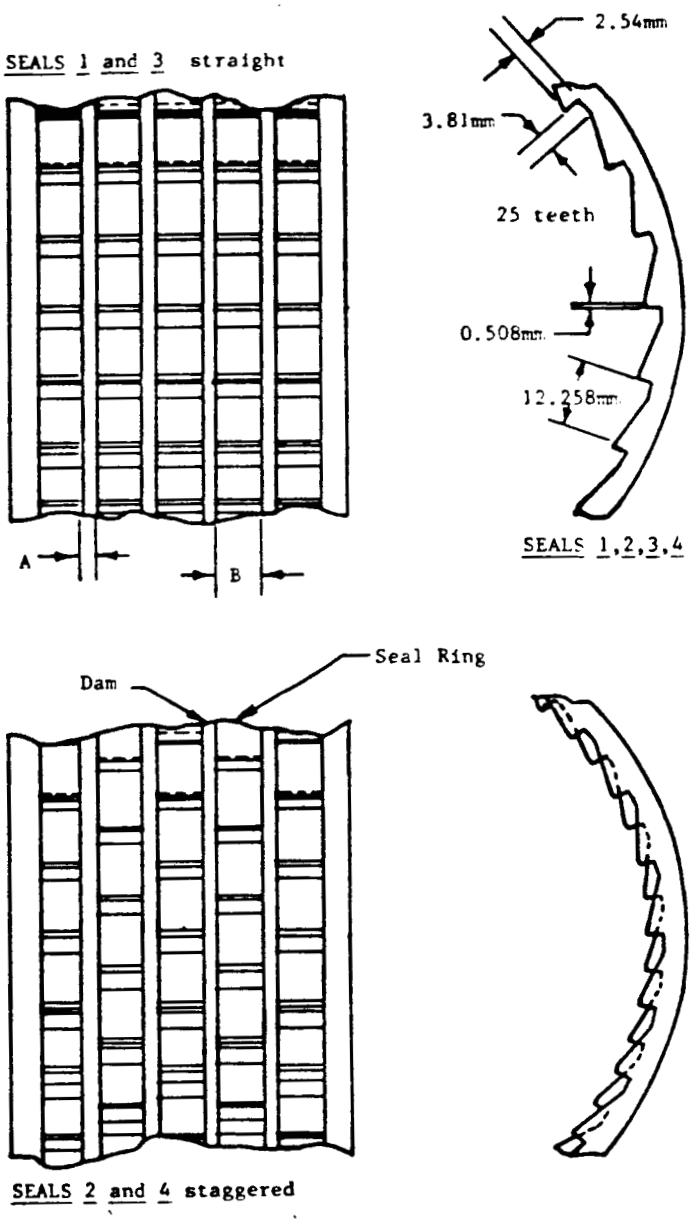

Fig. 5 Schematic for sawtooth-pattern stators 1 through 4

ORIGINAL PAGE IS
OF POOR QUALITY

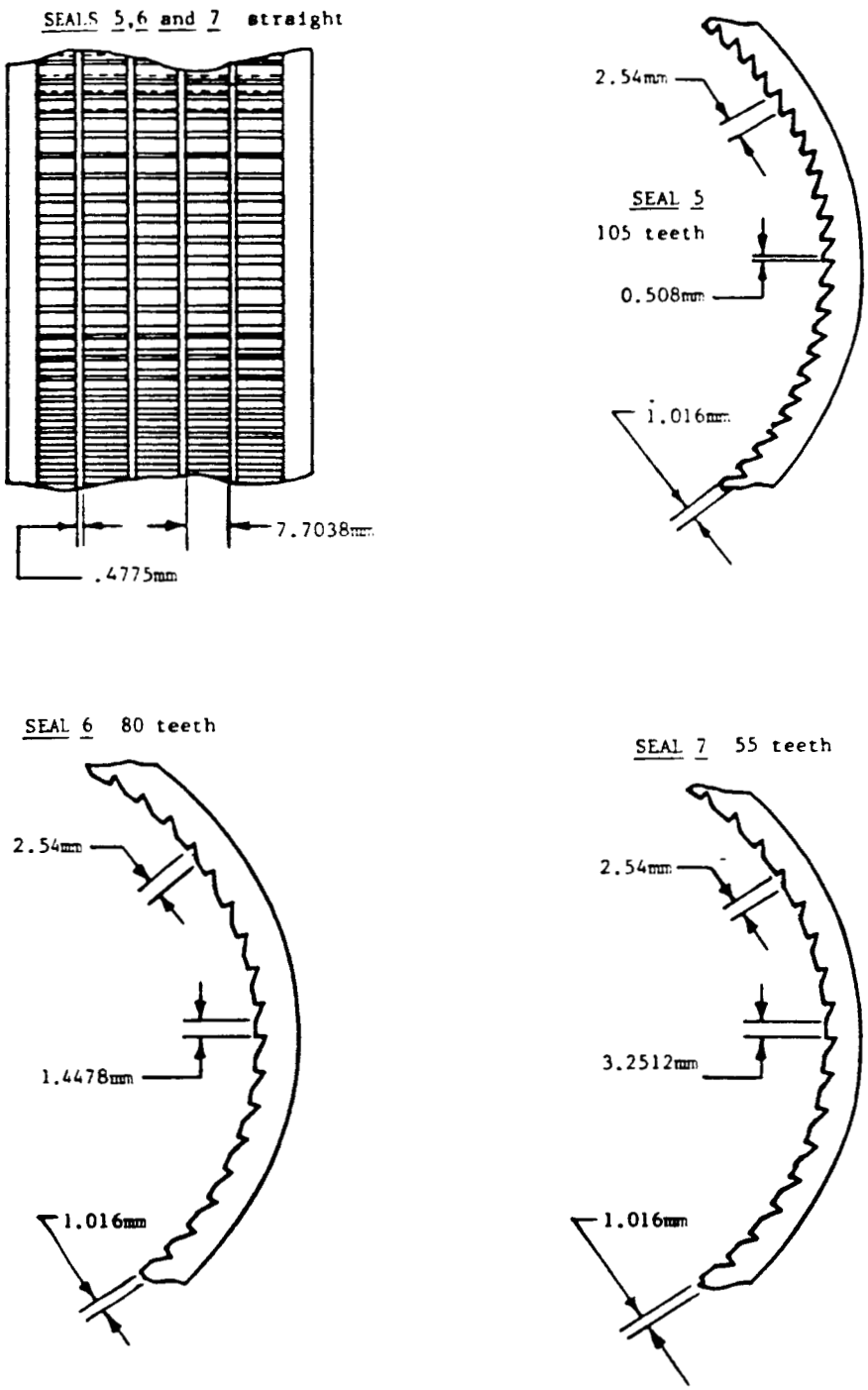

Fig. 6 Schmatic for sawtooth-pattern stators 5 through 7

ORIGINAL PAGE IS
OF POOR QUALITY

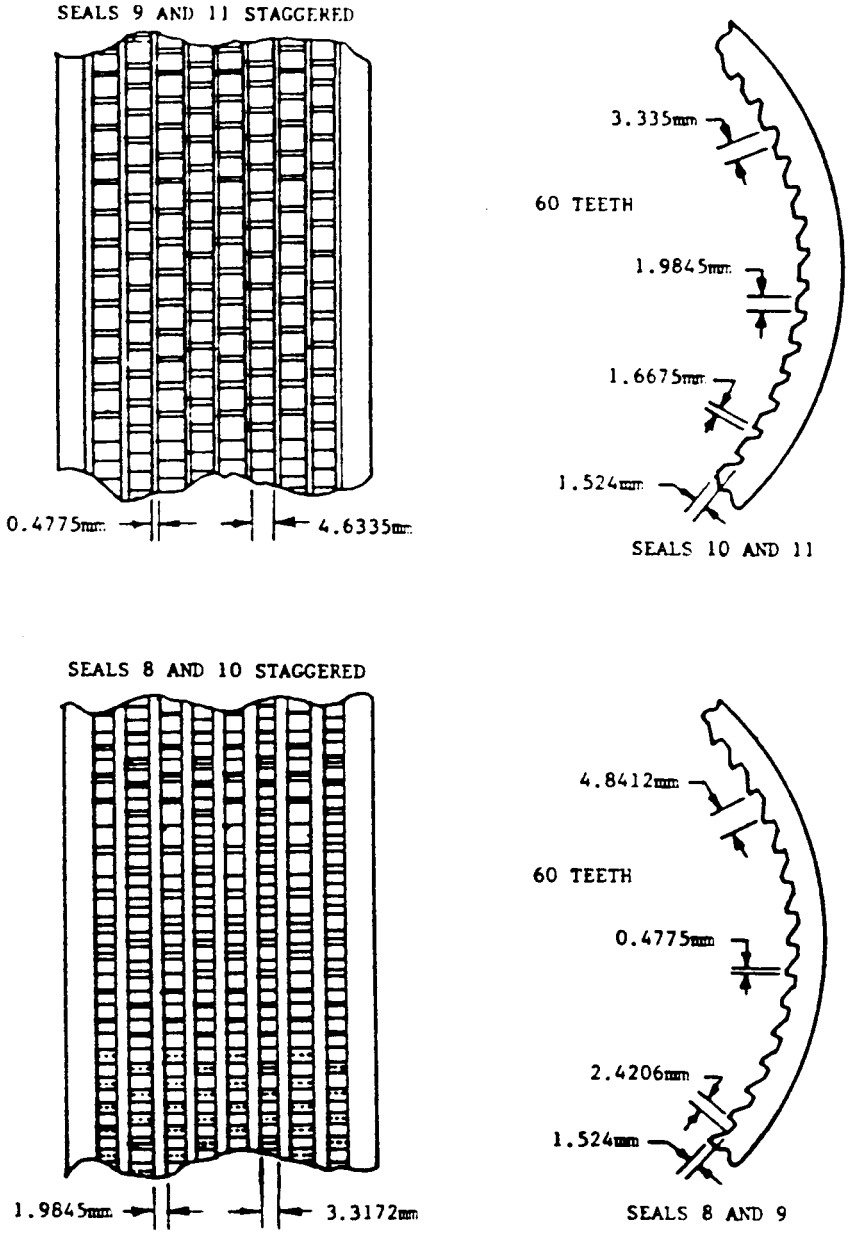

Fig 7 Schematic for sawtooth-pattern stators 8 through 11

configurations, rotordynamic coefficients, consisting of effective stiffness, effective damping, and mass coefficients are extracted from their F_r/A and F_θ/A data. The following procedure is used to extract these coefficients.

If the displacement of the rotor is assumed to be a circular orbit of the form

$$X = A \cos\omega t \qquad Y = A \sin\omega t$$

then equation (1) yields the following definition of force coefficients which are, respectively, parallel and normal to the rotating displacement vector.

$$F_r/A = -K - c\omega + M\omega^2$$

$$F_\theta/A = k - C\omega \tag{2}$$

These equations sugest that all of the coefficients can be obtained by testing at three different running speeds. However, because the cross-coupled coefficients, c and k, are linear functions of ω [3], this approach is impossible. Additionally, for a long seal with equal rotor and stator roughness, the asymptotic circumferential fluid velocity is $R\omega/2$ and theory [3] predicts that $k = C\omega/2$ and $c = M\omega$. The present test apparatus does not provide any intentional prerotation of the fluid so the variation of c and k with ω is expected to be of the form

$$k = b_1 C\omega/2 \ , \ b_1<1$$
$$c = b_2 M\omega \ , \ b_2<1 \qquad (3)$$

where b_1 and b_2 are nondimensional constants. Substitution of Eq. (3) into Eq. (2) yields

$$F_r/A = -K + M(1-b_2)\omega^2 = -K_{ef} + M_{ef}\ \omega^2$$
$$F_\theta/A = -C(1-b_1/2)\omega = -C_{ef}\ \omega \qquad (4)$$

The "net damping coefficient", C_{ef}, results from the drag force, $C\omega A$, and the forward whirl excitation force, kA. By curve fitting the data values for F_r/A and F_θ/A, the running speed dependency is eliminated, and values for effective stiffness, K_{ef}, damping, C_{ef}, and mass, M_{ef}, can be obtained. It is evident from Eq. (4) that K_{ef} is the zero-running speed intercept of the curve for F_r/A versus ω, and C_{ef} is the slope of the curve for F_θ/A versus ω.

For leakage performance the conventional discharge-coefficient definition

$$\Delta P = C_d \frac{\rho V^2}{2}$$

is used. Substituting this into the equation for the flow rate yields

$$Q = 2\pi R C_r V = \left(\frac{Cr}{R}\right) C_d^{-1/2} \cdot 2\pi R^2 \sqrt{\frac{2\Delta p}{\rho}}$$

From a rotordynamics viewpoint,the values obtained for C_{ef} and K_{ef} can be used for a direct comparison of the different stator configurations. These values will also be used for comparing the seal characteristics to theoretical predictions. The leakage performance of the seals will be compared by using the nondimensional leakage coefficient $C_d^{-1/2}$.

The test program and theoretical analysis for the sawtooth-pattern damper seals was designed to answer the following questions:

(a) How do changes in sawtooth geometry affect the stiffness, damping, and leakage characteristics of the sawtooth-pattern seals?

(b) How does the stiffness, damping, and leakage performance of the sawtooth seals compare to those of the hole-pattern damper seal and smooth seal?

(c) How well does the analysis of Childs and Kim predict the seal characteristics of the sawtooth-pattern seals?

CHAPTER III

TEST RESULTS: RELATIVE PERFORMANCE OF SEALS

The relative seal performance is evaluated by comparing the coefficients K_{ef} and C_{ef} obtained from the measured values for F_r/A and F_θ/A as described in the preceding chapter. The leakage performance is evaluated by a comparison of the values of $C_d^{-1/2}$. The leakage data for sawtooth-pattern seals 1, 2, and 3 is limited due to problems with the original vortex flowmeters which yielded invalid data at the higher Reynolds-numbers. These flowmeters were replaced between the testing of seals 3 and 4 with turbine flowmeters which provided reliable flow-rate data.

Since eleven seals were tested, the seals are compared in groups depending on their groove depth. In addition, results for a smooth seal and the optimum hole-pattern damper seal are included for comparison of the sawtooth-pattern seal performance.

Sators 1 through 4. Stators 1 through 4 have similar geometries with a h/C_r value of 4.8. A curve fit of the F_r/A and F_θ/A yields the values plotted for C_{ef} and K_{ef} of Figs. 8 and 9 which are used for seal comparison. It is evident from the curves of Fig. 8 that the damping performance for these deeply grooved seals is, at best, comparable to that of a smooth seal and significantly inferior to the optimum damper seal. It is also apparent that the damping coefficient for this group of seals is not greatly affected by the value of γ. The values for K_{ef}

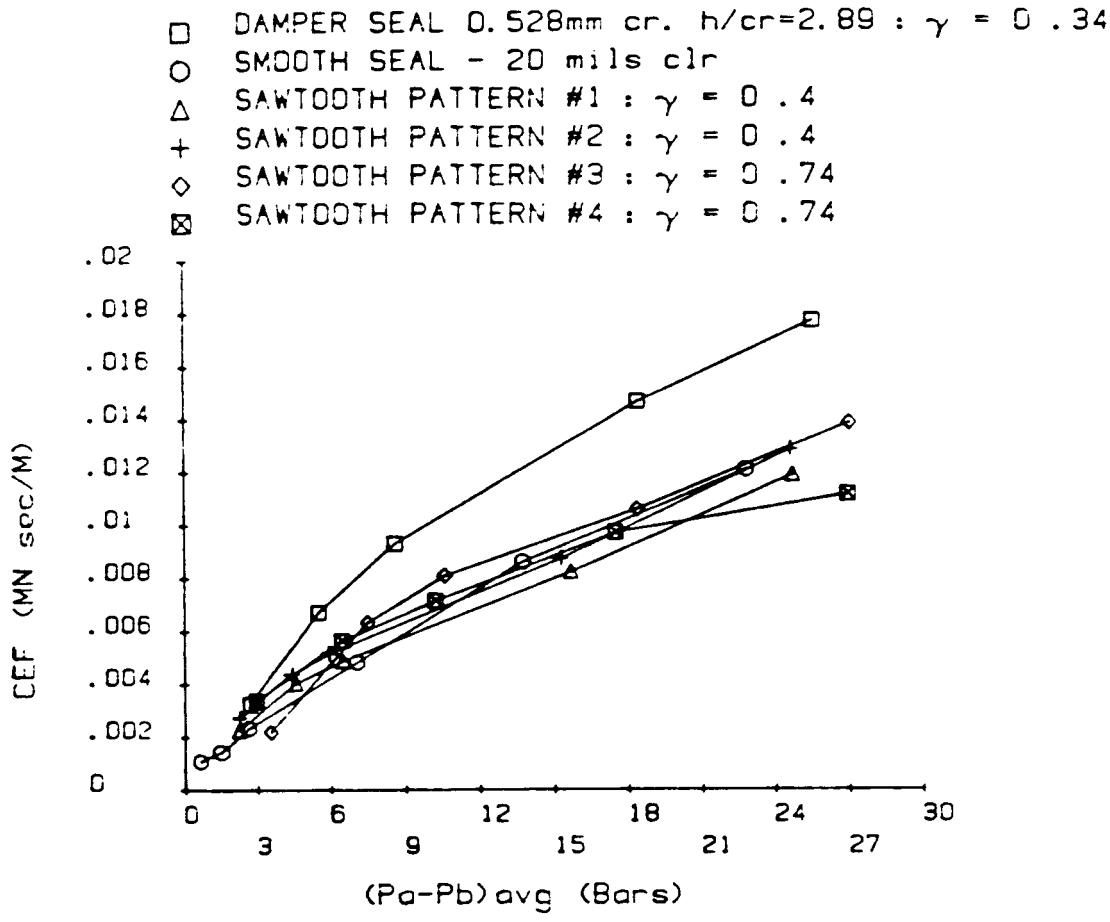

Fig. 8 C_{ef} **for sawtooth stators 1 through 4, optimum hole-pattern damper seal and a smooth seal**

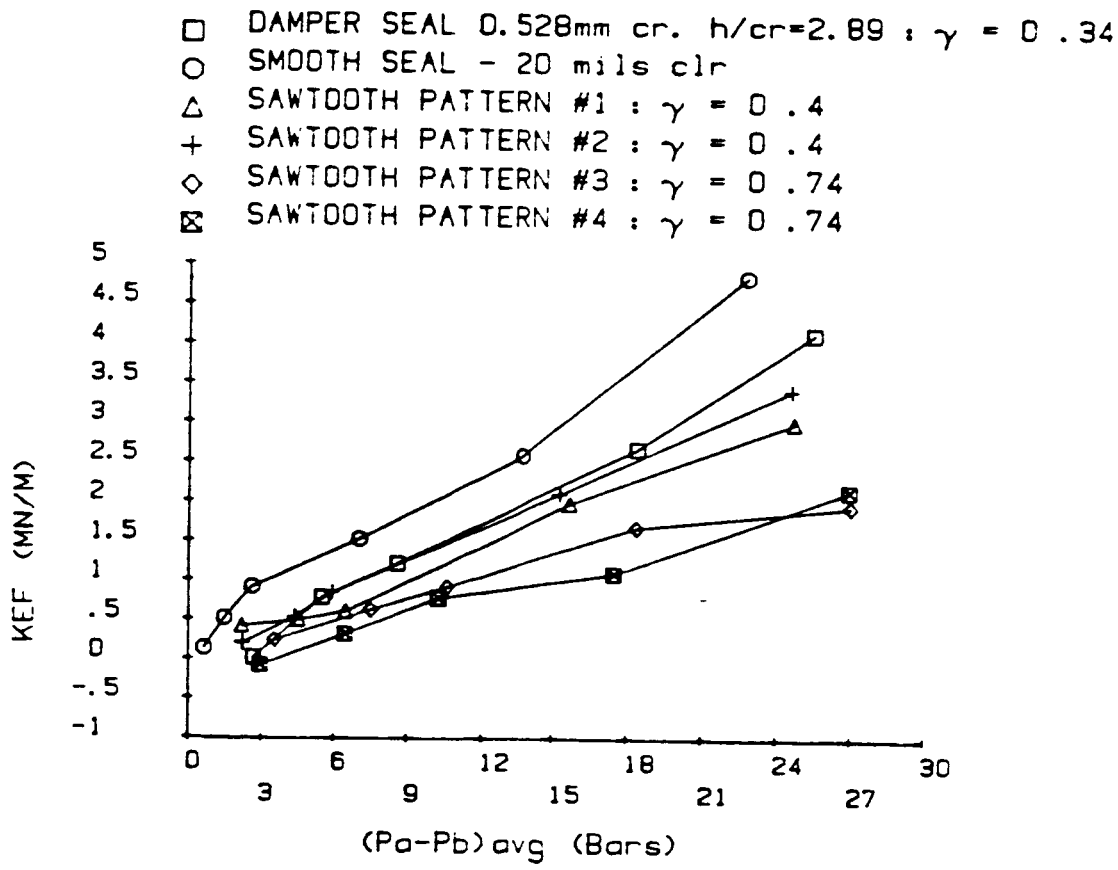

Fig. 9 K_{ef} for sawtooth stators 1 through 4, optimum hole-pattern damper seal and a smooth seal

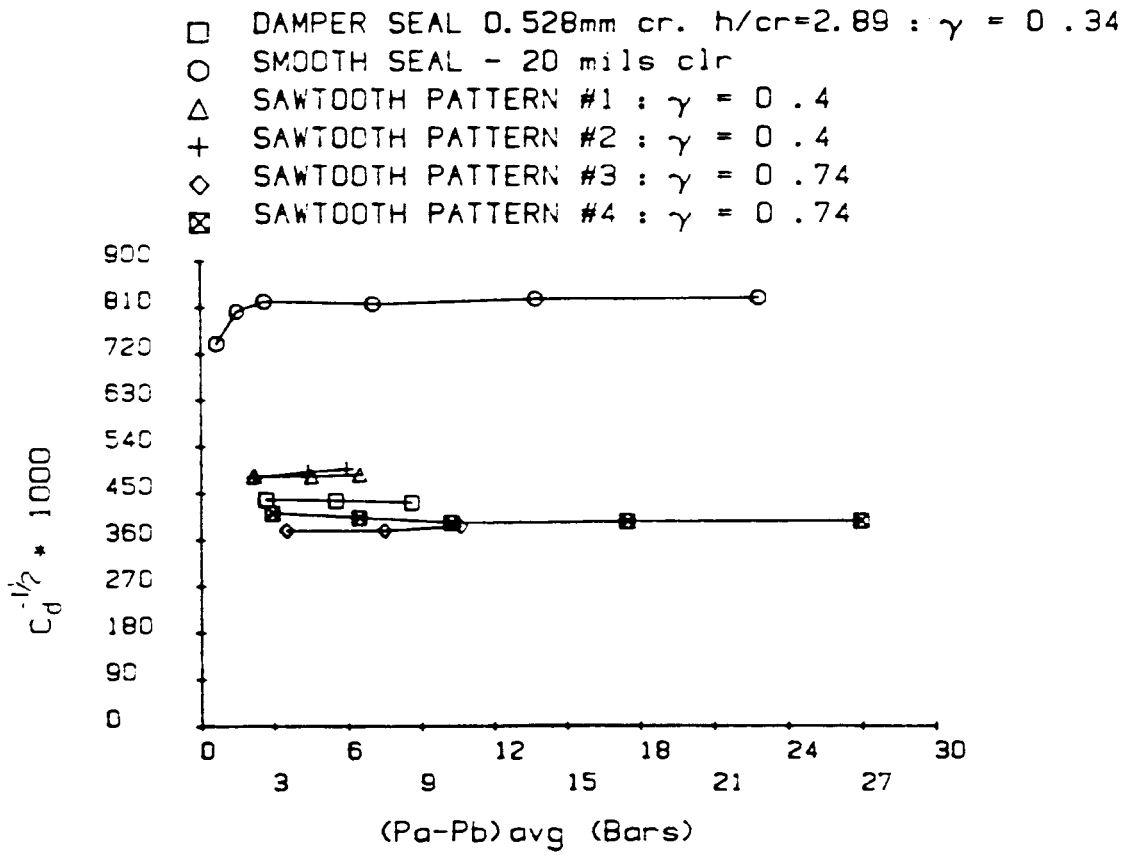

Fig. 10 $C_d^{-1/2}$ for sawtooth stators 1 through 4, optimum hole-pattern damper seal and a smooth seal

plotted in Fig. 9 show that this group of seals has significantly lower stiffness values than the smooth seal and generally lower values than the hole-pattern damper seal. Additionally, the values for K_{ef} are seen to depend on the value of γ. The increase of the hole area lowers the stiffness coefficient. Test results for the hole-pattern seals [12] showed a consistent drop in K_{ef} as γ is increased. Note also that the seal performance did not appear to change much when the sawtooth alignment was changed from straight to staggered.

The leakage data for seals 1 through 4 is shown in Fig. 10. All of the sawtooth-pattern seals leak much less than the smooth seal. However, stators 1 and 2 leaked more than the damper seal while seals 3 and 4 leaked less. Once again, the alignment of the sawteeth did not influence the seal performance.

Stators 5 through 7. This group of seals has an h/C_r=1.9 as well as the same groove geometry. The cross section of stator #5 coincides with the original sawtooth-pattern seal of [13]. These stators only differ in the number of teeth in the cross section which produces a consequent variation in γ.

The coefficients shown in Fig. 11 again show damping comparable to the smooth seal but substantially inferior to that of the hole-pattern seal. The damping coefficient is seen to be independent of the value of γ for this group of seals. The values of the stiffness coefficient of Fig. 12 tend to be a little erratic but generally similar to those of the hole-pattern seal. The stiffness values are all lower than the smooth seal and ignoring, what appear to be erratic data points, relatively independent of γ as well.

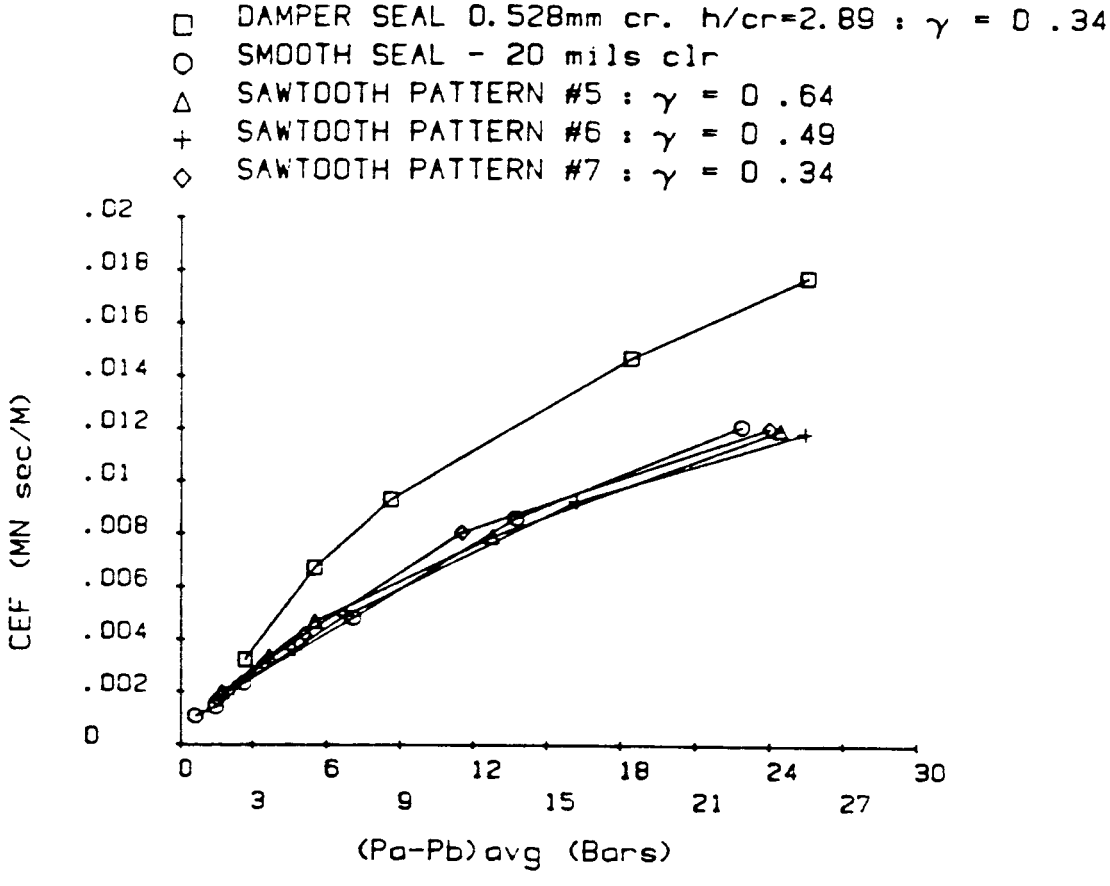

Fig. 11 C_{ef} for sawtooth stators 5 through 7, optimum damper seal and a smooth seal

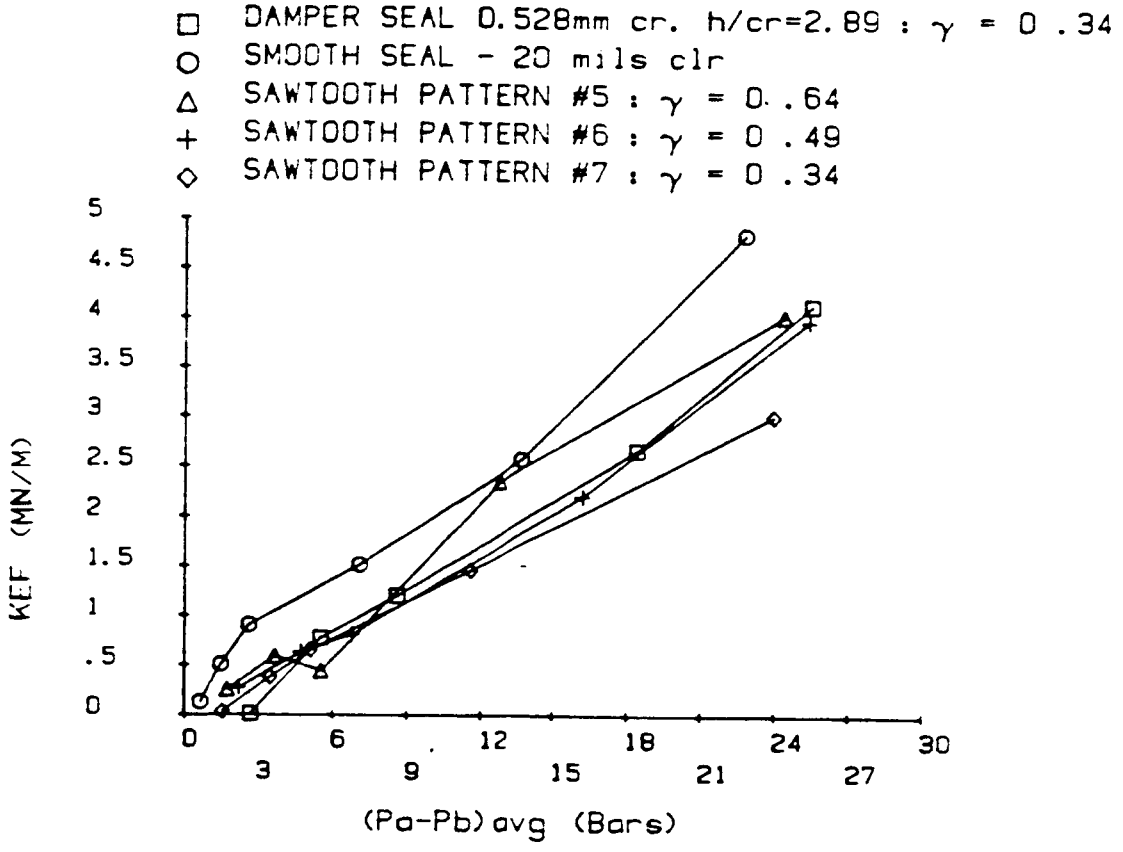

Fig. 12 K_{ef} for sawtooth stators 5 through 7, optimum damper seal and a smooth seal

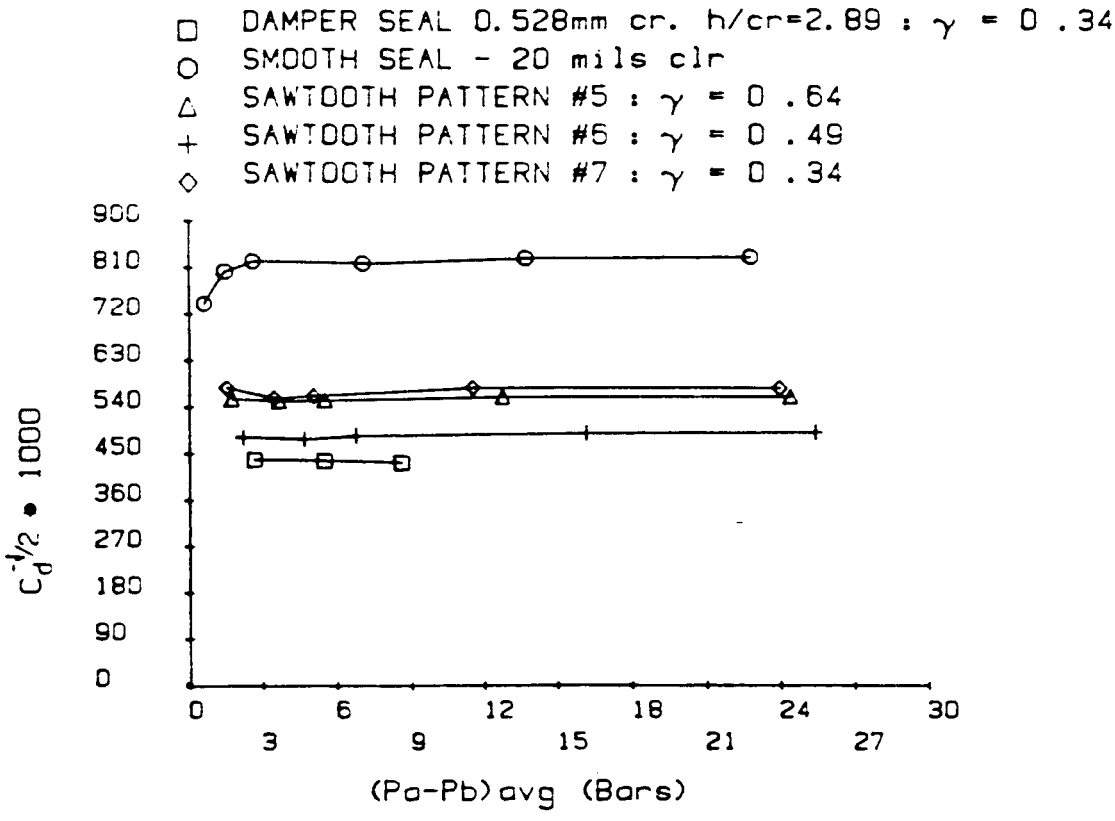

Fig. 13 $C_d^{-\frac{1}{2}}$ for sawtooth stators 5 through 7, optimum hole-pattern damper seal and a smooth seal

The leakage data in Fig. 13 show that these sawtooth-pattern seals leak less than the smooth seal but more than the best hole-pattern damper seal.

Stators 8 through 11. The test results for the dynamic data of stators 8 through 11 were curve fitted to obtain the coefficients presented in Figs. 14 and 15. These stators are again grouped together due to similar groove geometries and a common value of h/C_r=2.9. These seal-designs were guided by experience from the hole-pattern seals, which showed that maximum damping resulted for h/C_r = 2.9 and γ = 0.34. As shown in Fig. 14, the seals in this group exhibit better damping than the smooth seal. None of the seals had damping characteristics as good as the optimum hole-pattern damper seal. The stiffness values for this group of stators are illustrated in Fig. 15. While stators 8, 9, and 11 have lower values for K_{ef} than the hole-pattern seal, stator 10 has generally higher K_{ef} values than the hole-pattern damper seal. All stators in this group have lower K_{ef} values than the smooth seal.

The leakage performance of these stators is illustrated in Fig. 16. Note that stators 8 and 11, γ=0.48 and γ=0.47 respectivly, had leakage comparable to that of the damper seal, γ=0.34. Also, stator 10, γ=0.33, leaked more than the hole-pattern seal while stator 9, γ=0.68, leaked less. Again, all sawtooth stators leaked less than the smooth seal.

Best relative performance. From a damping viewpoint, none of the sawtooth-pattern seals provided damping performance as good as the optimum hole-pattern damper seal. The maximum effective damping performance was achieved by seals #10 (γ=0.33, h/C_r=2.9) and seal #11

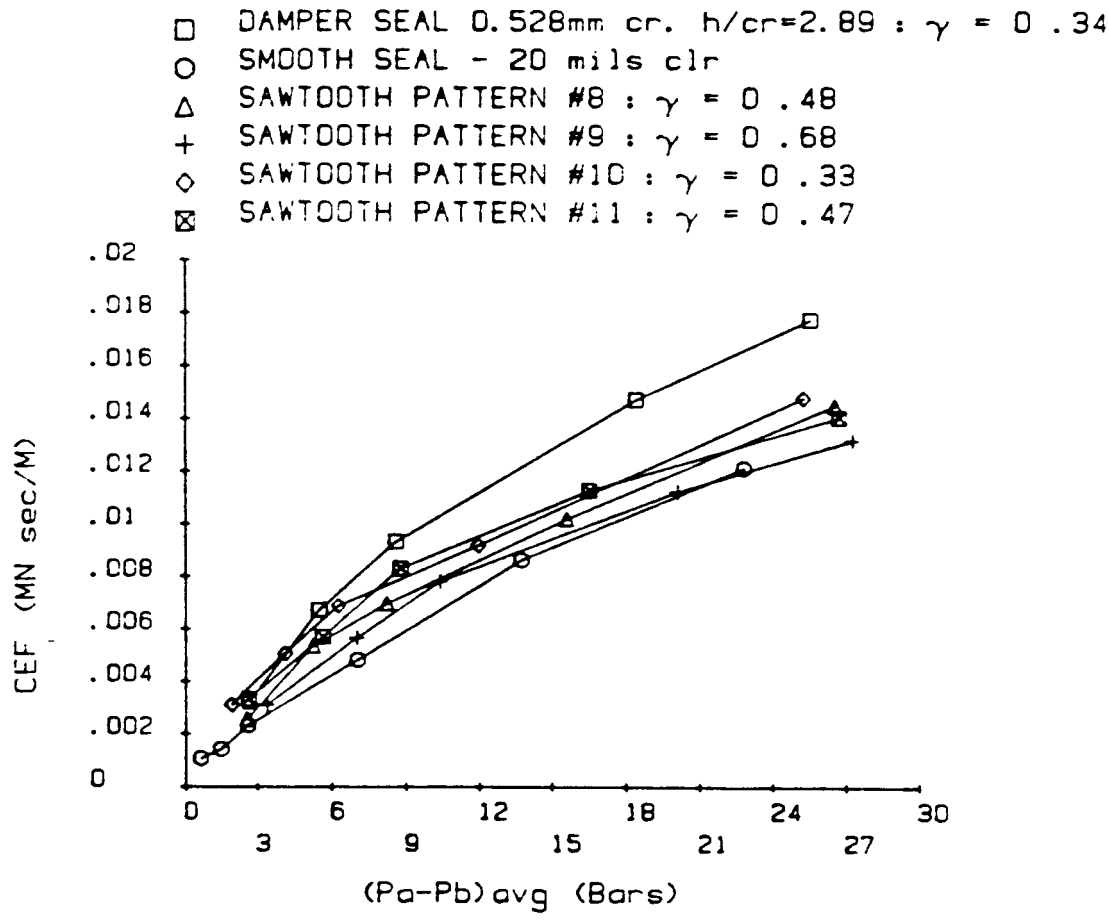

Fig. 14 C_{ef} for sawtooth stators 8 through 11, optimum hole-pattern damper seal and a smooth seal

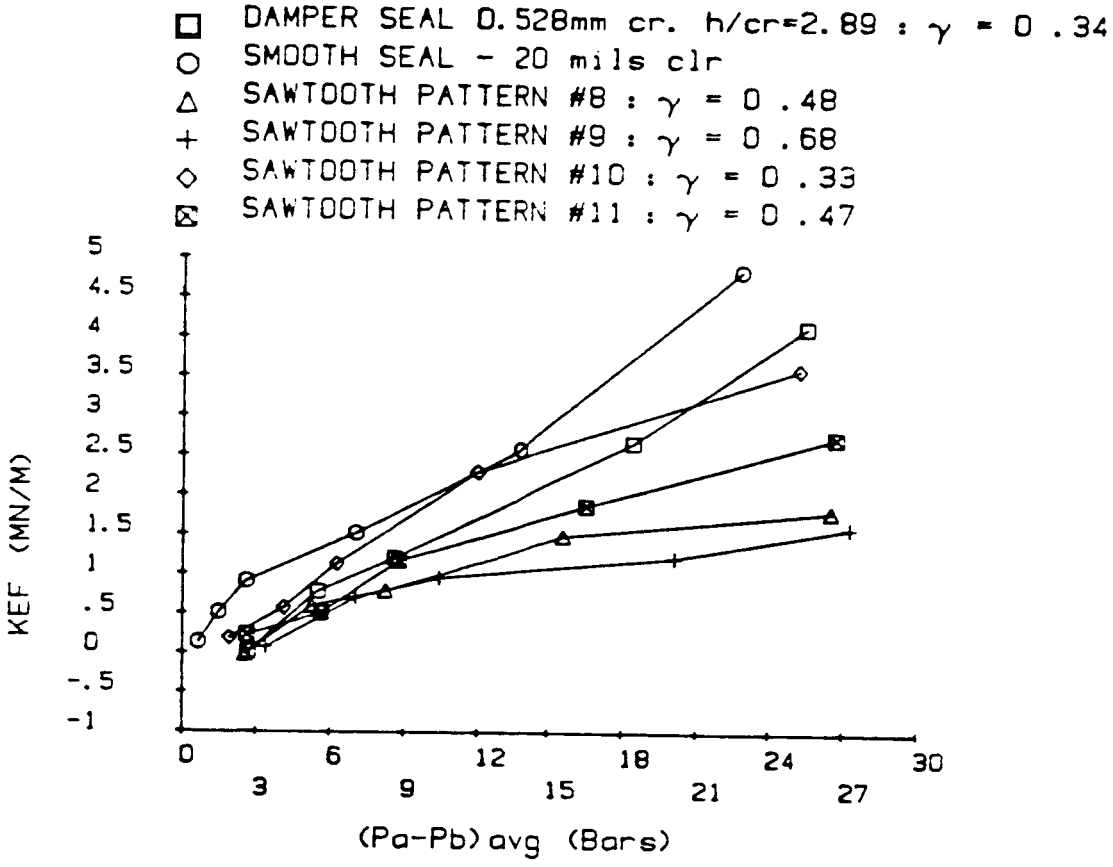

Fig. 15 K_{ef} for sawtooth stators 8 through 11, optimum hole-pattern damper seal and a smooth seal

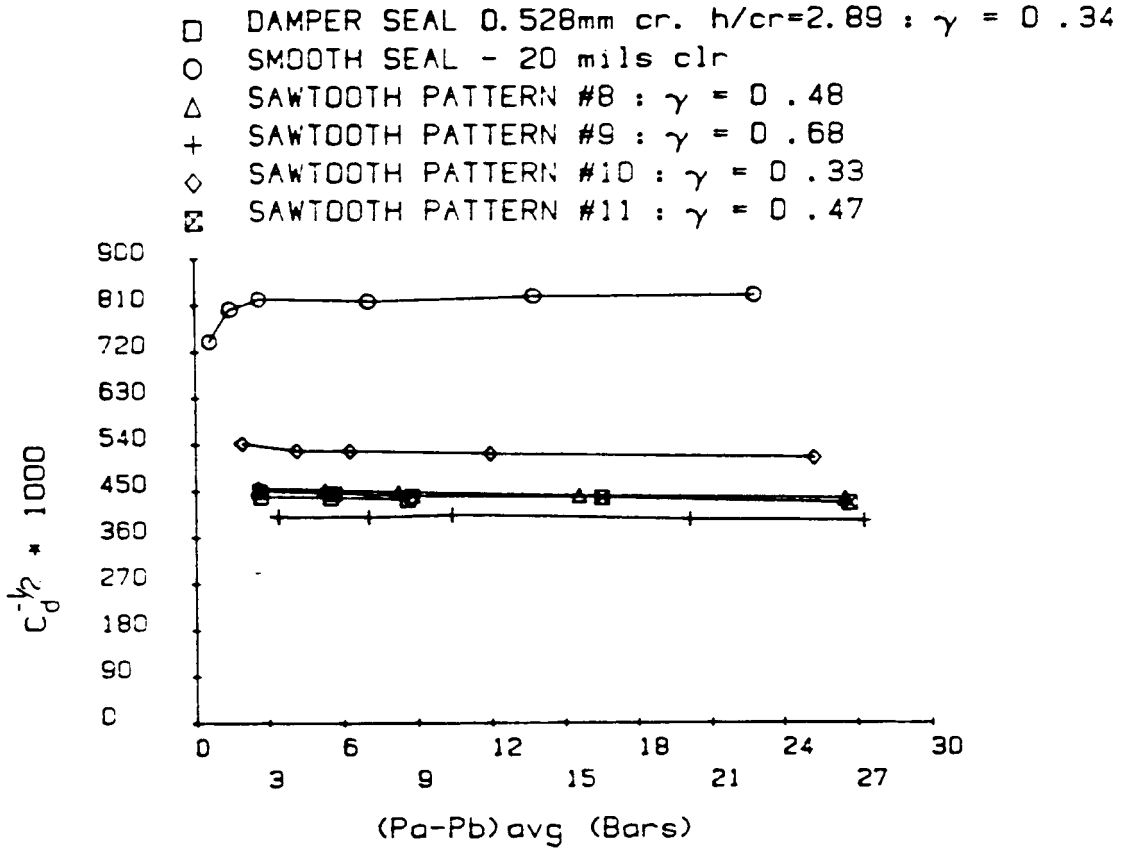

Fig.16 $C_d^{-1/2}$ for sawtooth stators 8 through 11, optimum hole-pattern damper seal and a smooth seal

(γ=0.47, h/C_r2.9); each of these seals provides a maximum damping performance at various values of ΔP, as seen in Fig. 14. The optimum hole-pattern damper seal provides 35 percent more net damping than a smooth seal as compared to an approximatley 18 percent increase for the best of the sawtooth-pattern damper seals

The sawtooth-pattern seals all had lower values of K_{ef} than the smooth seal. Two stators, stators #5 (γ=0.33, h/C_r=1.9) and #10 (γ=0.33, h/C_r=2,9) , provided the maximum K_{ef} values for the sawtooth seals.

All eleven sawtooth-pattern seals had significantly lower leakage rates than the smooth seal. The best leakage performance was provided by seals #3 and #4 (γ=0.74, h/C_r=4.9) and #9 (γ=0.68, h/C_r=2.9). These three seals had approximately equal values for $C_d^{-1/2}$, which were lower than the hole-pattern damper seal.

The sawtooth-pattern seal which provided the best characteristics, from the rotordynamics viewpoint of maximizing C_{ef} and K_{ef}, was stator #10. However, note from Fig. 16 that it leaked considerably more than the optimum damper seal . It is interesting to note that this stator has almost exactly the same parameters as the optimum hole-pattern damper seal, with γ = 0.33 and h/C_r = 2.9.

CHAPTER IV

ANALYSIS

An analysis for turbulent annular seals with different, directionally-homogeneous surface-roughness treatments for rotor and stator elements was developed by Childs and Kim [11]. Their analysis is based on slight modifications to Hirs' [9] governing equations and uses a perturbation procedure which is basically that of reference [7]. Although the sawtooth-pattern seals do not rigidly conform to the condition of having a directionally homogeneous surface roughness, this analysis will be used to make a theoretical comparison to several of the sawtooth seals that have surface roughness patterns which are approximately homogeneous.

A differential fluid element, with upper and lower surfaces corresponding to the rotor and stator surfaces respectively, is shown in Fig. 17. The bulk fluid velocities, which are averages across the film hight $H(\theta,t)$, of the axial and circumferential fluid velocities, are U_z and U_θ. Hirs' turbulence formulation is based on an empirical function for the wall shear stress, τ_w, of the form

$$\tau_w = \rho \frac{V_w^2}{2} n_o R_a^{mo}$$

where

$$R_a = \frac{2\rho V_w H}{\mu}$$

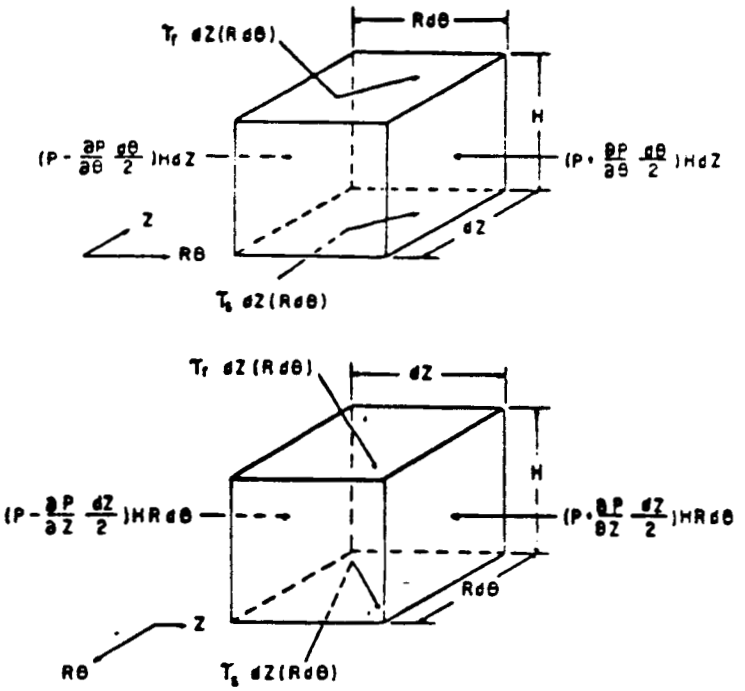

Fig. 17 Differential fluid element

and V_w is the average bulk-flow velocity relative to the wall. For the same surface roughness on the stator and rotor surface, the empirical coefficients m_o and n_o apply to both surfaces. For different surface roughnesses on the rotor and stator, the wall shear stresses are respectively

$$\tau_r = \rho \frac{V_r^2}{2} n_r \left(\frac{2\rho V_r H}{\mu}\right)^{m_r}$$

$$\tau_s = \rho \frac{V_s^2}{2} n_s \left(\frac{2\rho V_s H}{\mu}\right)^{m_s} \qquad (5)$$

with bulk flow velocities relative to the rotor and stator

$$V_r = (U_\theta - R\omega)\, \varepsilon_\theta + U_z\, \varepsilon_z$$

$$V_s = U_\theta\, \varepsilon_\theta + U_z\, \varepsilon_z$$

Using the above definitions for the shear-stress, governing equations consisting of axial and circumferential momentum equations are developed. The bulk flow continuity equation completes the governing equations.

These governing equations define the bulk-flow velocity components and the pressure as functions of the spatial variables, $R\theta$ and Z, and the time. Using a perturbation technique the nondimensional variables of these equations (u_z, u_θ, p and h) are expanded into zeroth-order and first-order equations. The zeroth-order equations can be solved for steady-state leakage, velocity fields and the pressure field. The

first-order equations define the rotordynamic coefficients.

For a constant clearance seal, the nondimensional zeroth-order equations are

$$\frac{dp_o}{dz} = -\left(a_{os}\,\sigma_s + a_{or}\,\sigma_r \right)/2$$

$$\frac{du_{\theta o}}{dz} = \left[a_{os}\,\sigma_s\,u_{\theta o} + a_{or}\,\sigma_r(u_{\theta o} - 1) \right] \tag{6}$$

where

$$a_{os} = \left[\frac{1 + (u_{\theta o}/bu_{zo})^2}{1 + (1/4b^2)} \right]^{\frac{ms+1}{2}}$$

$$a_{or} = \left[\frac{1 + [(u_{\theta o}-1)/bu_{zo}]^2}{1 + (1/4b^2)} \right]^{\frac{mr+1}{2}}$$

Since the zeroth-order equations are coupled and nonlinear their solution is iterative. The initial conditions for these two nonlinear equations are

$$p(0) = \Delta P \,/\, \rho V^2$$

$$u_{\theta o} = U_{\theta o} \,/\, R\omega \tag{7}$$

<u>Empirical turbulence coefficients.</u> The analysis of Childs and Kim [11] characterizes the surface roughness of the stator and rotor in terms of empirical coefficients (n_s, m_s, n_r, m_r). These are the same coefficients

that appear in Eq. 5. These coefficients must be determined from static test data before the theoretical predictions can be made for F_r/A and F_θ/A. The coefficients can be calculated in the following manner.

The steady-state axial pressure gradient can be stated as

$$-\frac{\partial p}{\partial z} = \sigma \frac{\rho V^2}{2}$$

Leakage is measured in the test apparatus, and the pressure is measured at five axial locations. Averages of the measured upstream and downstream temperature and pressure are used to define the density. So, for known values for the density, axial velocity, and the measured pressure gradient, the parameter σ can be determined. The pressure gradient is determined from a curve fit of the three middle pressure locations so entrance end exit effects do not significantly influence the calculation. The three locations are at approximately 20, 50, and 80 percent of the seal length. For a rough-stator/smooth-rotor combination this value is σ_c, which is related to the stator, σ_s, and rotor, σ_r, by

$$\sigma_c = \frac{\sigma_r + \sigma_s}{2} \tag{8}$$

The σ parameters are related to the friction factor, λ, by

$$\sigma_r = \lambda_r \frac{L}{C} \quad , \quad \sigma_s = \lambda_s \frac{L}{C} \tag{9}$$

and the friction factor is related to the empirical coefficients through the following friction-factor formulas

$$\lambda_r = n_r \, Ra^{mr} \, [1 + ((u_\theta - 1)/b)^2]^{\frac{mr+1}{2}} \tag{10}$$

$$\lambda_s = n_s \, Ra^{ms} \, [1 + (u_\theta/b)^2]^{\frac{ms+1}{2}} \tag{11}$$

where

$$b = V/R\omega$$

This leads to the following problem which must be resolved: given measured data sets (Ra_i, ω_i, λ_i), determine the values for m_r, n_r, m_s, and n_s from Eqs. (10) and (11).

The tangential velocity component, u_θ, of Eqs. (10) and (11) is generally a function of the axial position z. In previous analyses, the value for u_θ has been set equal to the constant asymptotic value for seals with equal rotor and stator roughnesses, viz., $u_\theta = 1/2$. For the present analysis u_θ is set equal to the average nondimensional circumferential velocity

$$\bar{u}_\theta = \int_0^1 u_\theta(z) \, dz \tag{12}$$

where $u_\theta(z)$ is the solution of the zeroth-order equations. Hence Eqs. (10) and (11) become

$$\lambda_r = n_r R_a^{mr} [1 + ((\bar{u}_\theta - 1)/b)^2]^{\frac{mr+1}{2}} \tag{13}$$

$$\lambda_s = n_s R_a^{ms} [1 + (\bar{u}_\theta/b)^2]^{\frac{ms+1}{2}} \tag{14}$$

Since the solution of the zeroth-order equations for u_θ and P_o depend on m_r, n_r, m_s, and n_s, the solution is iterative. To begin the iterative solution procedure, a value must be assumed for $u_{\theta o}(0)$. Once this value is assumed, first approximations for m_r, n_r, m_s, and n_s can be calculated from Eqs. (13) and (14). Experience shows that for the present apparatus, $u_{\theta o}(0) = 0.1$ is an adequate approximation.

For a smooth stator and smooth rotor the same coefficients apply for both rotor and stator; hence, $m_s = m_r$, and $n_s = m_s$, so n_r and m_r can be found for the smooth-rotor/smooth-stator data. The parameter-identification procedure is slightly different when both surfaces have the same roughness, as apposed to the smooth rotor/rough stator combination, and a more detailed explanation is provided first.

From Eq. (8)

$$\sigma_c = \frac{L}{2C} (\lambda_r + \lambda_s) \tag{15}$$

For the same roughness on both surfaces, the empirical coefficients n and m are the same , and Eq. (15) can be stated

$$2\sigma_c \frac{C}{L} = 2\lambda_c = n (C_1 X^m + C_2 Y^m) \tag{16}$$

where

$$C_1 = [\ 1 + ((u_\theta - 1)/b)^2\ ]^{1/2}$$

$$C_2 = [\ 1 + (u_\theta/b)^2\ ]^{1/2} \qquad (17)$$

$$X = R_a C_1\ ,\quad Y = R_a C_2\ ,$$

This form of the governing equations isolates the unknown coefficients m and n.

Previously, the circumferential velocity u_θ was assumed to be the asymptotic velocity of 1/2 which makes $-C_1=C_2$ and $X=-Y$, and a linear curve fit of the log form of Eq.(16) yields ln(n) and m. However, if u_θ is not equal to 1/2, $-C_1$ is not equal to C_2, and performing the logarithm of Eq. (16) will not linearize the problem.

In the following procedure, u_θ is set equal to $\overline{u}_\theta$ in Eq. (17). The parameters m and n are defined by minimizing the following objective function

$$E = \sum_{i=1}^{k} (2\lambda_{ci} - 2\hat{\lambda}_{ci})^2 = \sum_{i=1}^{k} [\ n(C_{1i}X_i^m + C_{2i}Y_i^m) - 2\hat{\lambda}_{ci}]^2 \qquad (18)$$

which is the summation over the k data points of the squared difference between the predicted, λ_{ci}, and the measured, $\hat{\lambda}_{ci}$, friction factors. Minimization of E with respect to m and n yields the following equations

$$f = \frac{\partial E}{\partial n} = \sum_{i=1}^{k} [\, n(C_{1i}X_i^m + C_{2i}Y_i^m) - 2\hat{\lambda}_{ci}](C_{1i}X_i^m + C_{2i}Y_i^m) = 0$$

$$g = \frac{\partial E}{\partial m} = \sum_{i=1}^{k} [\, n(C_{1i}X_i^m + C_{2i}Y_i^m) - 2\hat{\lambda}_{ci}]\; n(C_{1i}X_i^m \ln X_i + C_{2i}Y_i^m \ln Y_i)m = 0 \qquad (19)$$

These nonlinear equations are solved for n and m using a Newton-Raphson procedure.

Figure 18 provides a flowchart for the solution algorithm used in obtaining n and m for equal rotor and stator roughnesses. An iterative solution is required since the differential equations (6) include the unknown parameters n and m, and Eq. (19) contains C_1 and C_2 which depend on $\bar{u}_\theta$.

The above procedure was used to calculate the following values for a seal with a smooth rotor and smooth stator.

$$m_r = -0.112 \qquad n_r = 0.0353 \qquad (20)$$

The seal tested had a four inch (101.6 mm) diameter with a 0.020 inch (0.508 mm) clearance.

A comparison between measured and predicted values for σ, based on these values, over a range of running speeds and Reynolds numbers is given in Fig. 19. Observe that the curve fit does a generally satisfactory job.

In the present investigation, we are interested in calculating empirical coefficients m_s and n_s for various surface roughened stators

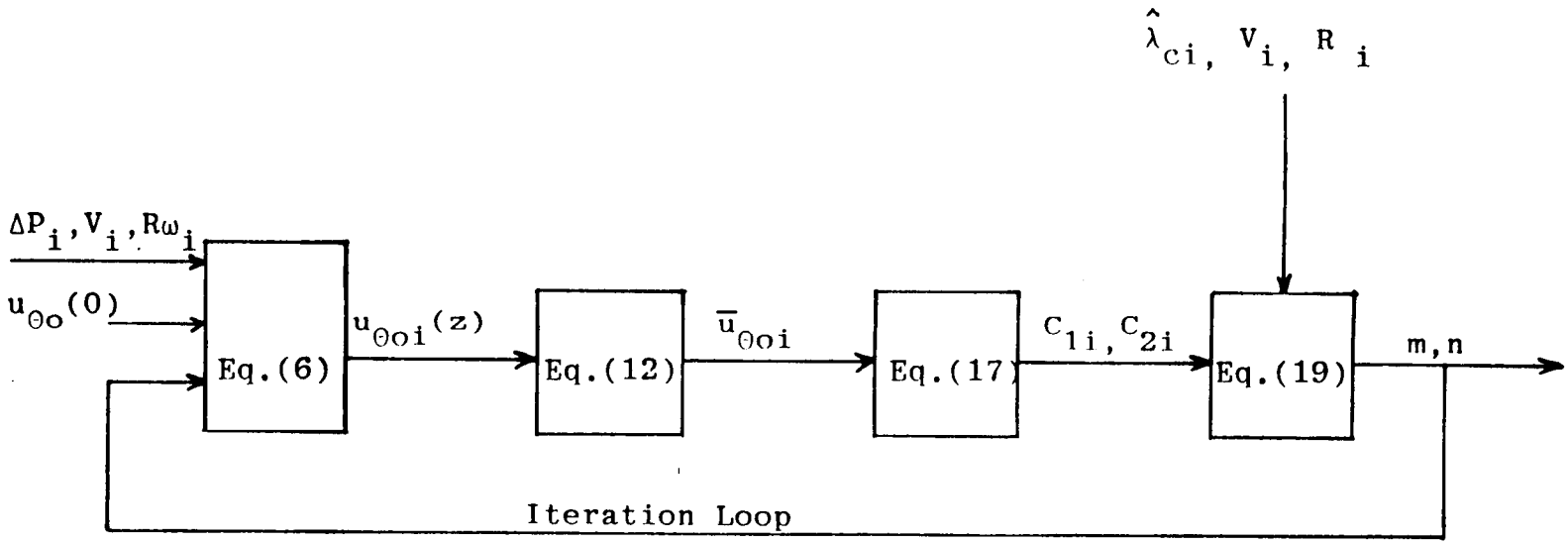

Fig. 18 Flowchart for the solution of the empirical coefficients for equal rotor and stator surface roughnesses. The subscript i denotes the ith data point.

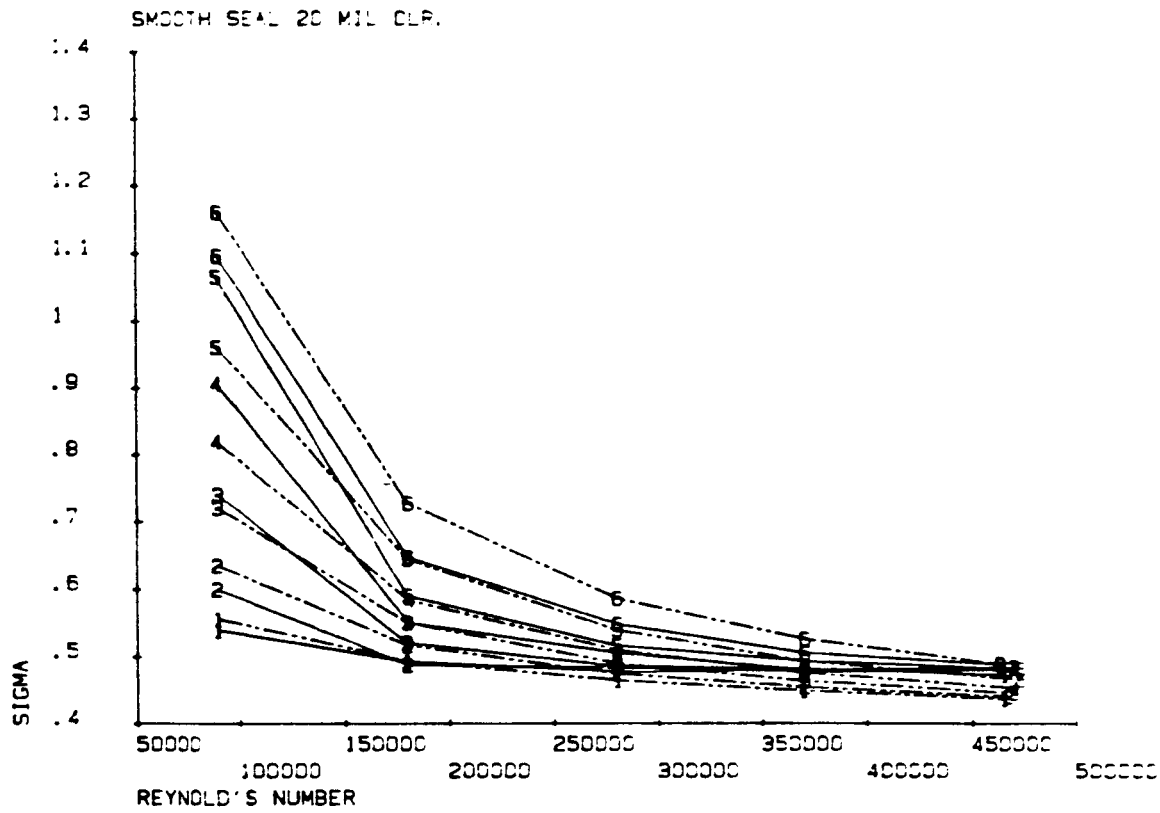

Fig. 19 Experimental and calculated values for σ based on calculated empirical coefficients for a smooth seal

assuming that values for m_r and n_r are known for the rotor. The values for m_r and n_r from Eq. (20) are used in the present study.

The flowchart of Fig. 20 illustrates the solution procedure for the values of m_s and n_s with known values for m_r and n_r. The upper portion of this figure shows the calculation of λ_{ri} from Eq. (13). Eq. (15) is then used to subtract λ_{ri} from the measured combined seal friction factor λ_{ci} to obtain a value for λ_{si}. For a given data point, Eq. (14) can be restated as

$$Z_i = \ln (n_s) + m_s X_i$$

where

$$Z_i = \ln\left(\frac{\lambda_{si}}{[1 + (\bar{u}_{\theta i}/b_i)^2]1/2}\right)$$

$$X_i = \ln(R_a [1 + (\bar{u}_{\theta i}/b_i)^2]^{1/2})$$

The objective function to be minimized with respect to $\ln(n_s)$ and m_s is

$$E = \sum_{i=1}^{k} (Z_i - \hat{Z}_i)^2$$

where Z_i and $\hat{Z}_i$ are the measured and predicted values for Z_i respectively. A least-square curve fit of this relationship yields the following equations

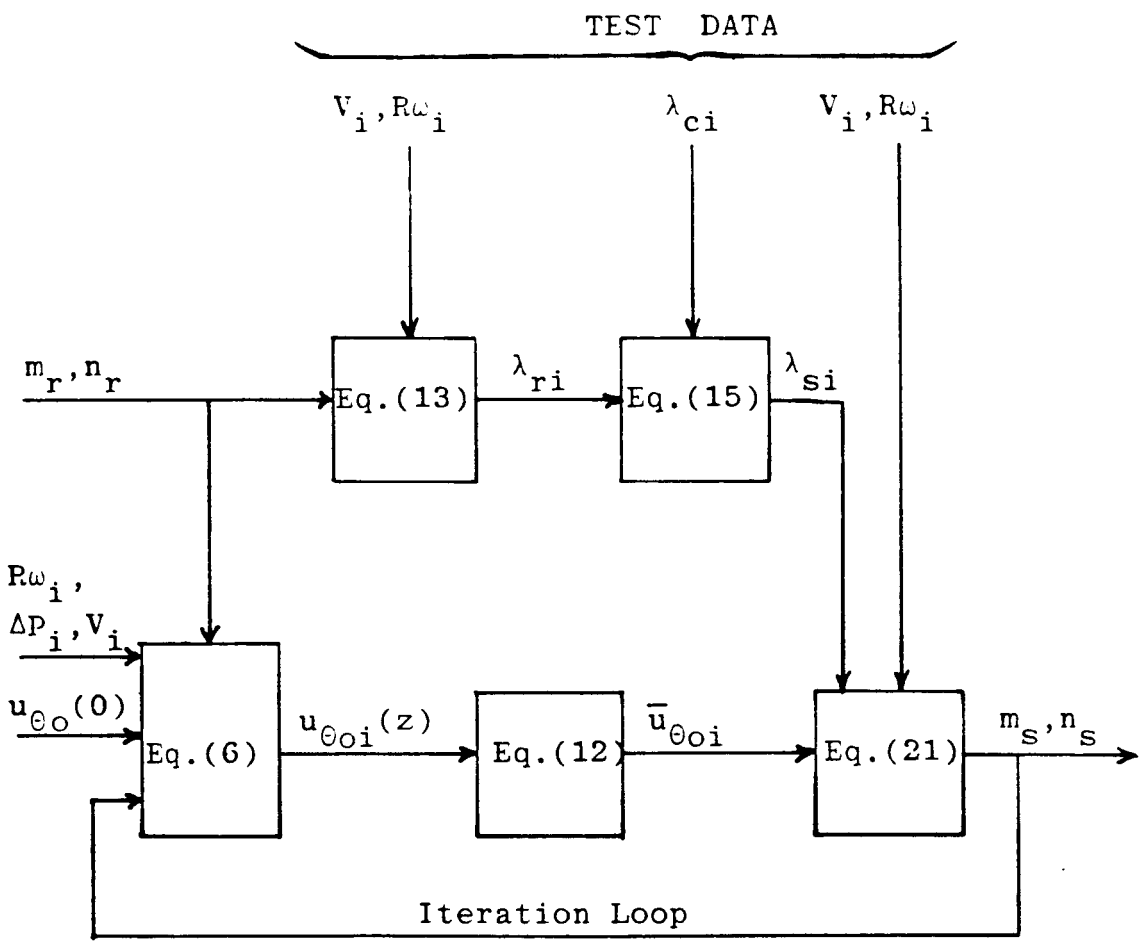

Fig. 20 Flowchart for the solution of stator empirical turbulence coefficients m_s, n_s from test data and known rotor coefficients. The subscript i denotes the ith data point

$$\begin{bmatrix} k & \sum_{i=1}^{k} X_i \\ \sum_{i=1}^{k} X_i & \sum_{i=1}^{k} X_i^2 \end{bmatrix} \begin{Bmatrix} \ln(n_s) \\ m_s \end{Bmatrix} = \begin{Bmatrix} \sum_{i=1}^{k} \hat{Z}_i \\ \sum_{i=1}^{k} X_i \hat{Z}_i \end{Bmatrix} \tag{21}$$

The resulting empirical coefficients are given in Table 2

Table 2. Empirical coefficients for stators 8 through 11

STATOR	m_s	n_s	Avg. % Diff for σ_{exp} vs. σ_{th}
# 8	0.0974	0.0279	9.9
# 9	0.0492	0.0747	7.5
# 10	-0.0428	0.1008	8.8
# 11	-0.0474	0.1971	8.8

These empirical coefficients are used in a computational method to obtain predictions for σ and for the radial and tangential force components to be used in the curve fit of Eq. 4. The experimental and theoretical predictions for σ are shown in Figs. 21 through 24. These figures show that even though the percent difference between the experimental and theoretical values for σ listed in Table 2 is less than ten percent for all four stators, the model does not do a good job of predicting the behavior of σ.

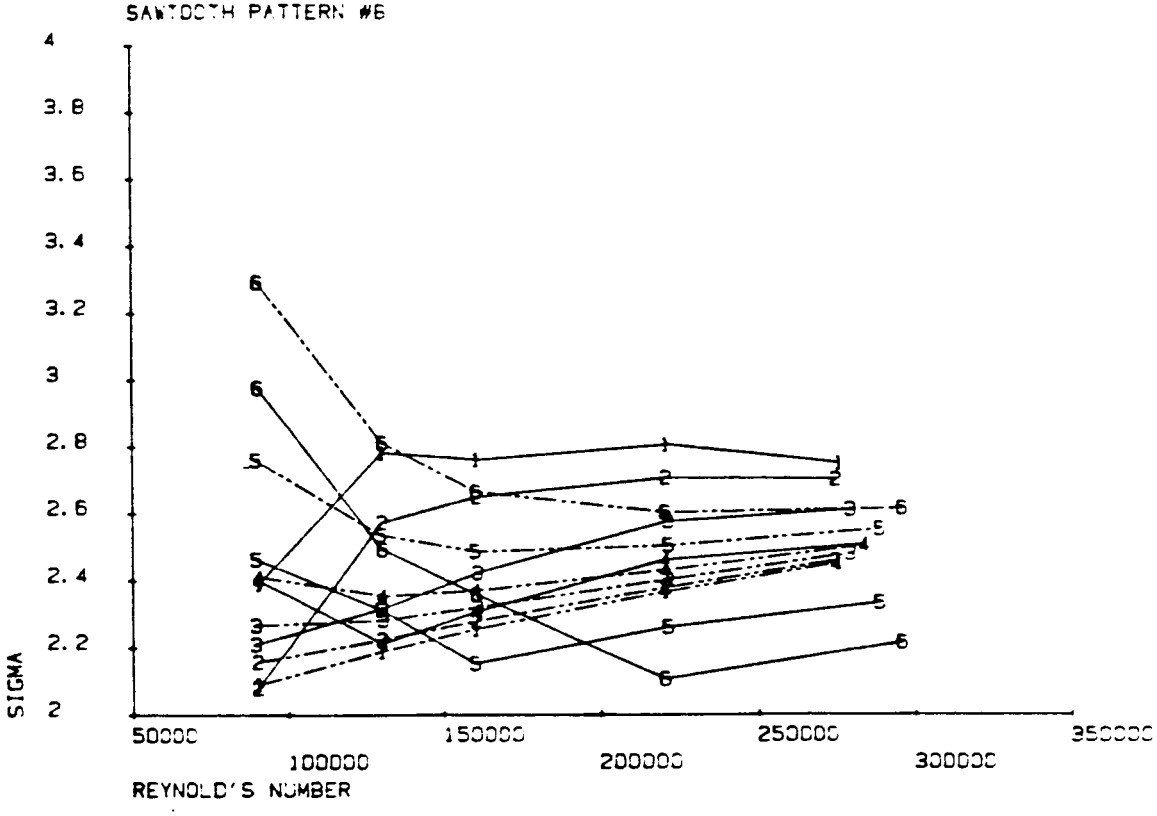

Fig. 21 Experimental and calculated values for σ for stator #8

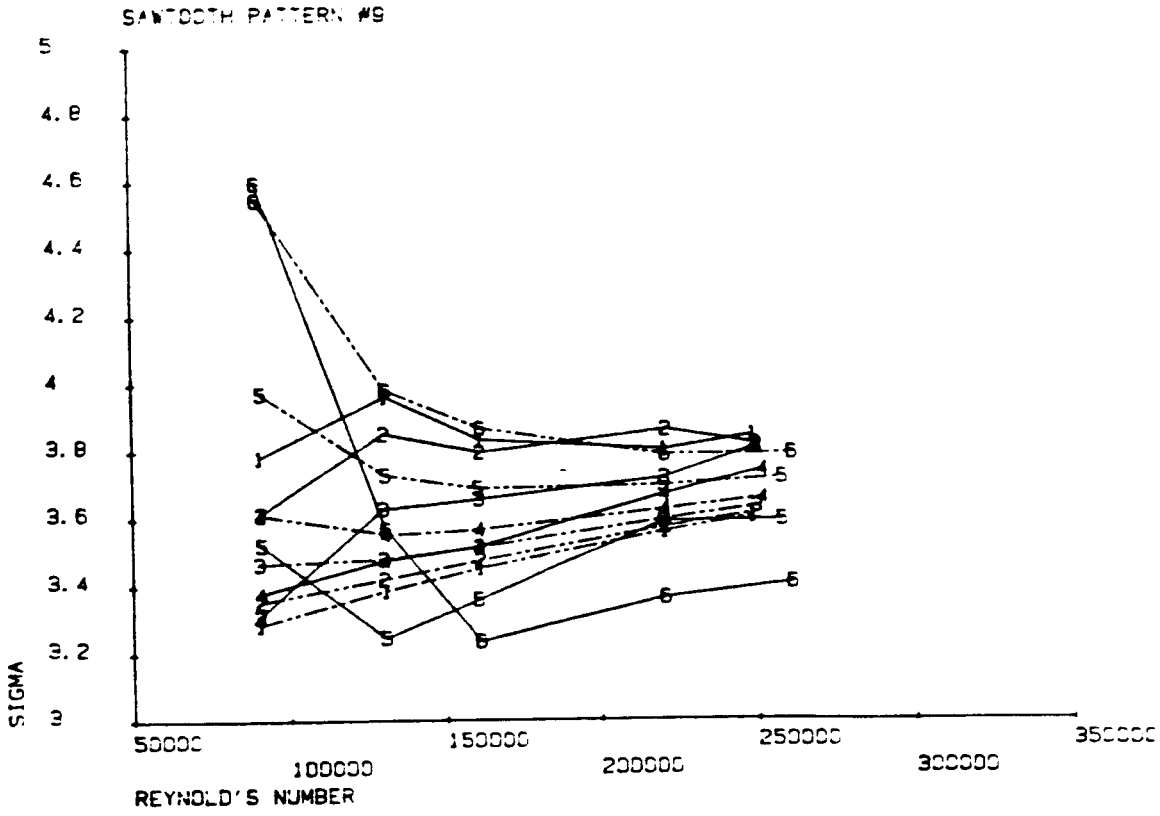

Fig. 22 Experimental and calculated values for σ for stator #9

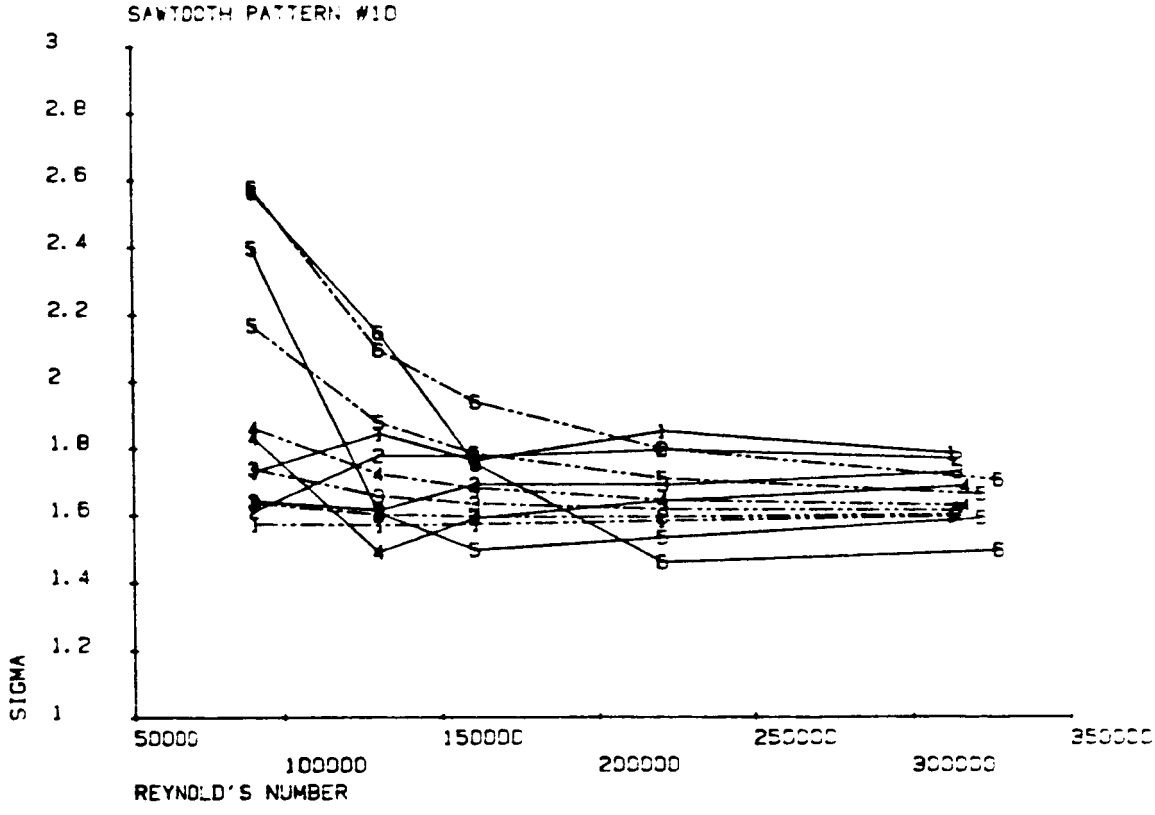

Fig. 23 Experimental and calculated values for σ for stator #10

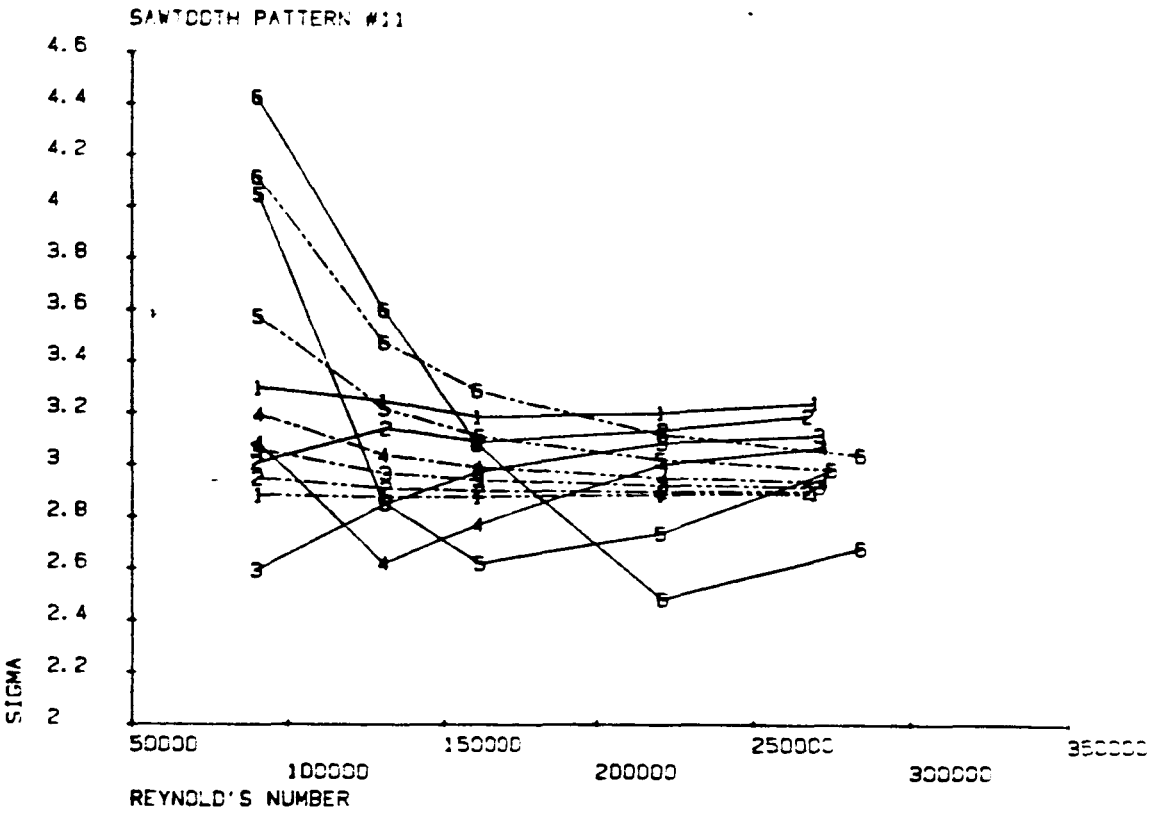

Fig. 24 Experimental and calculated values for σ for stator #11

The positive values of m_s obtained for stators # 8 and # 9 are unexpected. The Reynolds-number relationship with the shear stress, and hence σ generally yields a decrease in σ with increasing Reynolds-number and subsequently negative m_s values. For the lower running speed curves, 1, 2, and 3 for stators # 8 and # 9 there is a definite increase in σ with Reynolds-number. These data suggest that, despite the high Reynolds-numbers, the flow is not fully developed in the seal. The influence of the lower running speed data produces the positive values of m_s for a curve fit of all the data points.

As noted, Figs. 21 through 24 show that σ has a running speed dependency. This running speed dependency is predicted by Eq. 17. For the low Reynolds-numbers, and hence lower u_θ values, the term u_θ/b becomes more significant as ω is increased, since $b=V/R\omega$. While some dependency is expected, the wide spread in the σ values for rough stators shows that the theory is not doing a good job of predicting σ. This deviation is not as apparent in the smooth stator data of Fig. 19 although the running speed dependency can still be observed.

CHAPTER V

THEORY VERSUS EXPERIMENT: FORCE COEFFICIENTS

Introduction. The theoretical predictions obtained using the analysis of Childs and Kim [11] were compared to the experimental test results for several of the sawtooth pattern seals. As described earlier, the sawtooth-pattern seals do not, strictly speaking, conform to the condition of having a directionally homogeneous surface roughness for which the analysis was developed. The last group of seals tested, stators 8 through 11, had staggered tooth patterns with approximately "square" holes which nearly approximate a homogeneous roughness. The analysis was applied and comparisons were made for this group of seals.

The comparisons which were examined were for experimental and theoretical values for the radial and tangential force components, as well as the experimental and theoretical predictions for the stiffness and damping coefficients. In order to carry out the force coefficient analysis, the empirical coefficients of each stator were determined according to the procedure described in the Analysis section of this report.

Dynamic data. For any given seal, a test matrix similar to the one used to obtain the experimental data is used to generate the set of values for F_r/A and F_θ/A. As a matter of convenience the values for the running speed and Reynolds number were taken to be the same as those for the experimental data.

Figures A1 Through A8 in Appendix A contain the experimental and

theoretical results for F_r/A and F_θ/A versus R_a and ω for sawtooth-patterns 8 through 11. Inspection of the results leads to some interesting observations. There is generally poor agreement between the tangential force components for all four stators at all Reynolds numbers tested. In all cases, the magnitude of the predicted radial force is much lager than the experimental value. It also appears that the predictions become worse as the value of γ increases. The best comparisons are those for stator # 10, γ = 0.33. For stators # 8 and # 11, γ = 0.48 and γ =0.47, the results tend to deviate slightly more. The results for stator # 9, γ = 0.68, are by far the worst with most of the predicted values being off by a factor of two. This result should probably be expected since as γ increases the sawtooth pattern deviates more from a homogeneous approximation.

The radial force predictions for these stators are much closer to the experimental values. The theoretical and experimental values compare fairly well at the lower running speeds and Reynolds numbers. As the running speed and Reynolds number are increased, however, the values begin to stray .

Rotordynamic coefficient comparison. For another important comparison between the theoretical predictions and experimental results, the rotordynamic coefficients obtained from the curve fit of the radial and tangential force data are tabulated in Tables 3, 4, and 5.

Examination of these tables provides some important information. It can be seen from Table 3 that the theory does an adequate job of predicting values for Kef. In general, the theory over predicts Kef at the lower Reynolds numbers and under predicts Kef at the higher

Table 3. Experimental and theoretical comparison of K_{ef} for stators 8 through 11

Stator	R_a	K_{ef} (N/M) Exp.	K_{ef} (N/M) Theory	K_{ef} (Ex/TH)
# 8	90,090	-20,900	151,000	-0.138
	129,900	597,000	338,000	1.76
	159,900	787,000	540,000	1.46
	220,000	1,490,000	1,060,000	1.41
	282,200	1,800,000	1,560,000	1.16
# 9	90,090	66,900	247,000	0.271
	130,100	695,000	510,000	1.36
	160,300	955,000	775,000	1.23
	219,900	1,220,000	1,390,000	0.877
	252,200	1,600,000	1,790,000	0.892
# 10	90,050	181,000	242,000	0.747
	129,800	571,000	651,000	0.877
	160,100	1,130,000	973,000	1.16
	219,800	2,290,000	1,570,000	1.46
	316,700	3,600,000	2,930,000	1.23
# 11	89,970	224,000	246,000	0.911
	130,000	504,000	601,000	0.838
	160,000	1,170,000	948,000	1.23
	220,100	1,870,000	1,670,000	1.12
	272,000	2,730,000	2,410,000	1.13

Table 4. Experimental and theoretical comparison of C_{ef} for stators 8 through 11

Stator	R_a	C_{ef} (N sec/M) Exp.	C_{ef} (N sec/M) Theory	C_{ef} (Ex/Th)
# 8	90,090	2,550	8,750	0.292
	129,900	5,340	9,460	0.565
	159,900	6,950	11,300	0.614
	220,000	10,200	14,800	0.690
	282,200	14,500	21,200	0.684
# 9	90,090	3,090	10,400	0.297
	130,100	5,630	12,700	0.445
	160,300	7,800	14,500	0.539
	219,900	11,200	20,700	0.543
	252,200	13,600	24,800	0.530
# 10	90,050	3,110	7,320	0.425
	129,800	5,060	9,040	0.560
	160,100	6,870	10,400	0.658
	219,800	9,160	13,100	0.699
	316,700	14,800	19,800	0.748
# 11	89,970	3,330	9,200	0.362
	130,000	5,690	11,000	0.518
	160,000	8,290	12,400	0.671
	220,100	11,300	16,800	0.671
	272,000	14,000	23,000	0.611

Table 5. Experimental and theoretical comparison of M_{ef} for stators 8 through 11

Stator	R_a	M_{ef} (Kg) Exp.	M_{ef} (Kg) Theory	M_{ef} (Ex/Th)
	90,090	7.93	4.27	1.86
	129,900	3.76	3.39	1.11
# 8	159,900	5.78	2.93	1.98
	220,000	7.13	2.42	2.94
	282,200	11.80	3.06	3.88
	90,090	6.84	3.62	1.89
	130,100	4.51	3.09	1.46
# 9	160,300	5.50	2.56	2.15
	219,900	11.5	2.37	4.84
	252,200	11.2	2.54	4.40
	90,050	7.40	3.79	1.95
	129,800	7.63	2.90	2.63
# 10	160,100	5.95	2.94	2.02
	219,800	5.29	4.45	1.19
	316,700	12.4	4.75	2.60
	89,970	9.012	3.484	2.59
	130,000	8.991	2.969	3.03
# 11	160,000	7.561	2.929	2.58
	220,100	9.716	2.835	3.25
	272,000	13.500	2.961	4.56

Reynolds-numbers. There is one exception to this. The values for stator # 9 are over predicted at the highest Reynolds numbers.

The theoretical predictions for the damping coefficients are much worse than for the stiffness. For all stators, the theory greatly over predicts the values of C_{ef}. The predictions for C_{ef} at the lowest Reynolds-numbers are the worst, but the predictions tend to improve as the Reynolds-number increases. None of the predictions are very good with the best being for stator # 10.

The theoretical values obtained for the values of M_{ef} are also not very good and are all under predicted. Most of the values for M_{ef} are off by almost a factor of two.

As a comparison for the quality of these predictions, previous results for a smooth seal and a hole pattern damper seal [12] are provided in Table 6. These results appear better for the predictions for the values of C_{ef} than those obtained for the sawtooth-pattern seals but worse for the predictions for K_{ef}. The M_{ef} values obtained are comparable for all three types of seals.

Table 6. A comparison of theoretical and measured values for stiffness, damping, and added-mass coefficients

Seal	R_a	K_{ef} (ex/th)	C_{ef} (ex/th)	M_{ef} (ex/th)
Smooth	120,100	2.182	0.6636	1.38
	170,600	2.216	0.6900	1.38
	270,500	1.297	0.7565	4.45
	385,200	1.142	0.9350	6.86
	495,700	1.261	0.9964	9.35
	500,900	1.478	0.9401	0.986
Hole-Pattern	89,410	1.573	0.4506	1.94
	130,400	1.768	0.6997	2.25
	159,700	1.876	0.7867	2.58
	328,400	2.175	1.205	1.88

CHAPTER VI

CONCLUSIONS

Testing of eleven sawtooth-pattern damper seals was carried out to obtain rotordynamic characteristics for each seal. Additionally the results for four of the seals were compared to predictions based on an analysis developed by Childs and Kim [11].

The experimental results and their comparison to theory support the following conclusions.

Experimental Results

(a) A sawtooth-pattern damper seal can be developed with much better damping and leakage performance than a corresponding smooth seal.

(b) The current data indicate that the best sawtooth-pattern seal is significantly inferior to the optimum hole-pattern seal previously developed, in terms of damping and leakage. The best sawtooth-pattern seal improves damping by 18 percent over the smooth seal as compared to almost 40 percent for the hole pattern and leaks approximately 20 percent more than the damper seal. Sawtooth stators 3, 4, and 9 leak less than the optimum hole-pattern seal.

(c) The sawtooth seal with the best overall rotordynamic performance, in terms of increased net damping and stiffness, has values of $h/C_r = 2.9$ and $\gamma = 0.33$, which are almost identical to the parameters for the optimum hole-pattern seal.

(d) The effective stiffness of the seals is decreased by

increasing γ and h/C_r.

(e) The leakage performance of the sawtooth-pattern seals is improved by increasing γ and h/C_r.

(f) There is no apparent advantage to using staggered, as opposed to aligned, sawtooth groove patterns.

Comparison to Theory

Due to the lack of a truly homogeneous surface roughness, the theory is not generally applicable to sawtooth-pattern damper seals; however, for the seals tested with an approximately directionally-homogeneous roughness, the following conclusions can be made:

(a) The theory does a fair job of predicting the effective stiffness values for the sawtooth-pattern seals, except at low Reynolds numbers where the predictions do not appear to be very accurate.

(b) The predictions for the net damping coefficients are generally greatly over predicted and not good.

(c) The added mass terms are always under predicted, usually by a very large percentage in excess of 50 percent.

(d) The theoretical values for the radial and tangential force components are not very good except at the lowest values of running speed.

REFERENCES

(1) Black, H. F., "Effects of Hydraulic Forces in Annular Pressure Seals on the Vibrations of Centrifugal Pump Rotors," J. Mech. Eng. Sci., Vol. 11, No. 2, 1969,pp. 206-213.

(2) Jenssen, D. N., "Dynamics of Rotor Systems Embodying High Pressure Ring Seals," Ph.D. dissertation, Hariot-Watt University, Edinburgh, Scotland, July 1970.

(3) Black, H. F. and Jenssen, D. N., "Dynamic Hybrid Properties of Annular Pressure Seals," Proc. Of J. Mech Eng., Vol. 184, 1970 pp. 92-100.

(4) Black, H. F. and Jenssen, D. N., "Effects of High-Pressure Ring Seals on Pump Rotor Vibrations," ASME Paper No.71-WA/FF-38, 1971.

(5) Childs, D. W., "The Space Shuttle Main Engine High-Pressure Fuel Turbopump Rotordynamic Instability Problem," ASME Trans J. of Eng. for Power, Jan. 1978, pp. 48-57.

(6) Lomakin, A. A., "Calculation of Critical Speed and Securing of Dynamic Stabilty of Hydraulic High Pressure Pumps with Reference to the Forces Arising in the Gap Seals," Energomashinostroeine, Vol. 4, 1958.

(7) Childs, D. W., "Finite-Length Solution for the Rotordynamic Coefficients of Turbulent Annular Seals," ASME Trans. J. of Lub. Tech., Vol. 105, Jul., 1983, pp. 437-444

(8) Childs, D. W., "Finite-Length Solution for the Rotordynamic Coefficients of Convergent-Tapered Annular Seals," 3rd

International Conference on Vibrations in Rotating Machinery, I MechE, London, England, 11-13, Sep., 1984.

(9) Hirs, G. G., "A Bulk Flow Theory for Turbulent Film Flow," J. of Lub. Tech., pp. 137-146, Apr., 1982.

(10) von Pragenau, G. L., "Damping Seals for Turbomachinery," NASA Technical Paper 1987, Mar., 1982.

(11) Childs, D. W. and Kim, C.-H., "Analysis and Testing for Rotordynamic Coefficients Of Turbulent Annular Seals with Different Directionally-Homogeneous Surface Roughness Treatments for Rotor and Stator Elements," ASME Transaction Journal of Tribology, Vol. 107, pp. 296-306, July 1985.

(12) Childs, D. W., and Kim, C.-H., "Test Results for Round-Hole-Pattern Damper Seals: Optimum Configuration and Dimensions for Maximum Net Damping," ASME Transaction Journal of Tribology, Vol. 108, pp.605-611, October 1986.

(13) Childs, D. W., "SSME HPFTP Interstage Seals: Analysis and Experiments for Leakage and Reaction Force Coefficients," Progress Report, NAS 8-33716, Texas A&M University-Turbomachinery Laboratories Report, Seal-1-83, 15 February 1983.

(14) Childs. D. W., "SSME HPFTP Interstage Seals: Analysis and Experiments for Leakage and Reaction-Force Coefficients," Supplementary Progress Report, NAS 8-33716, Texas A&M University-Turbomachinery Laboratories Report, Seal-2-83, 15 July 1983.

(15) Stephan, K., and Lucas, K., Viscosity of Dense Fluids, Plenum Press, New York-London, pp. 59, 1979.

APPENDIX A

EXPERIMENTAL AND THEORETICAL RESULTS FOR RADIAL AND TANGENTIAL FORCE COEFFICIENTS FOR STATORS 8 THROUGH 11

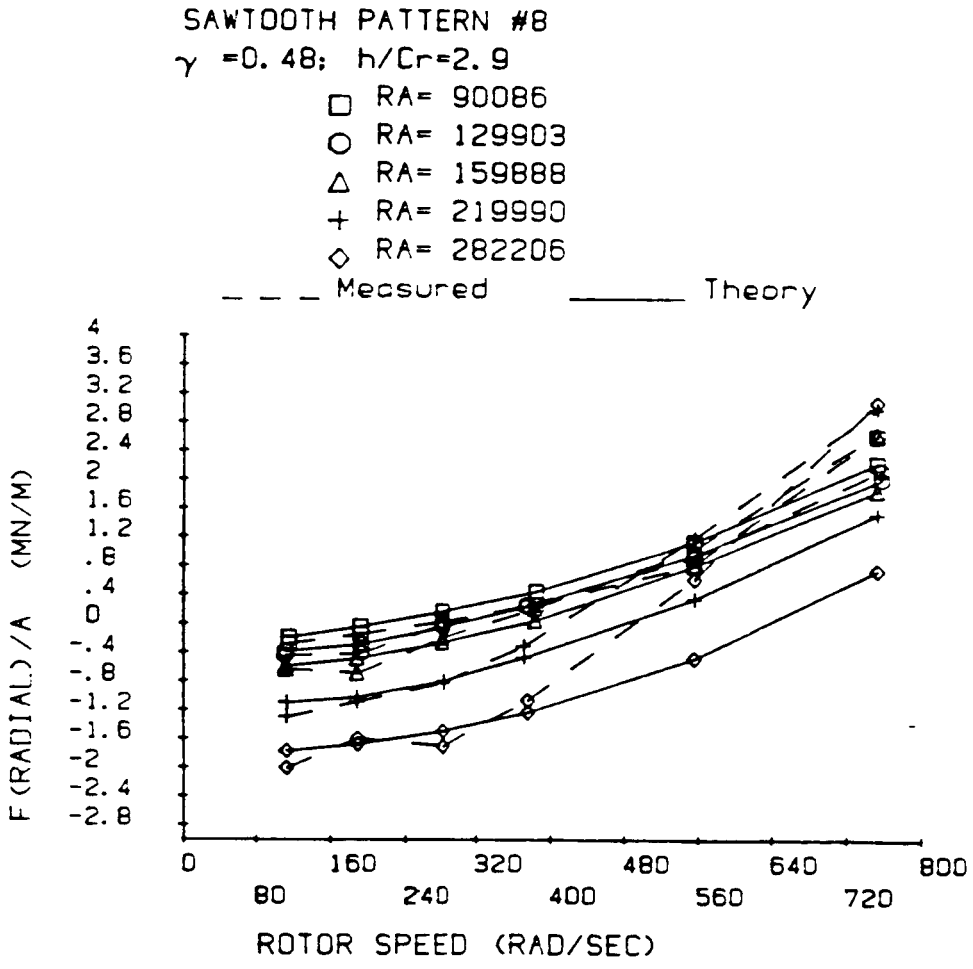

Fig. A1 Experimental and theoretical results for radial force coefficients for stator 8

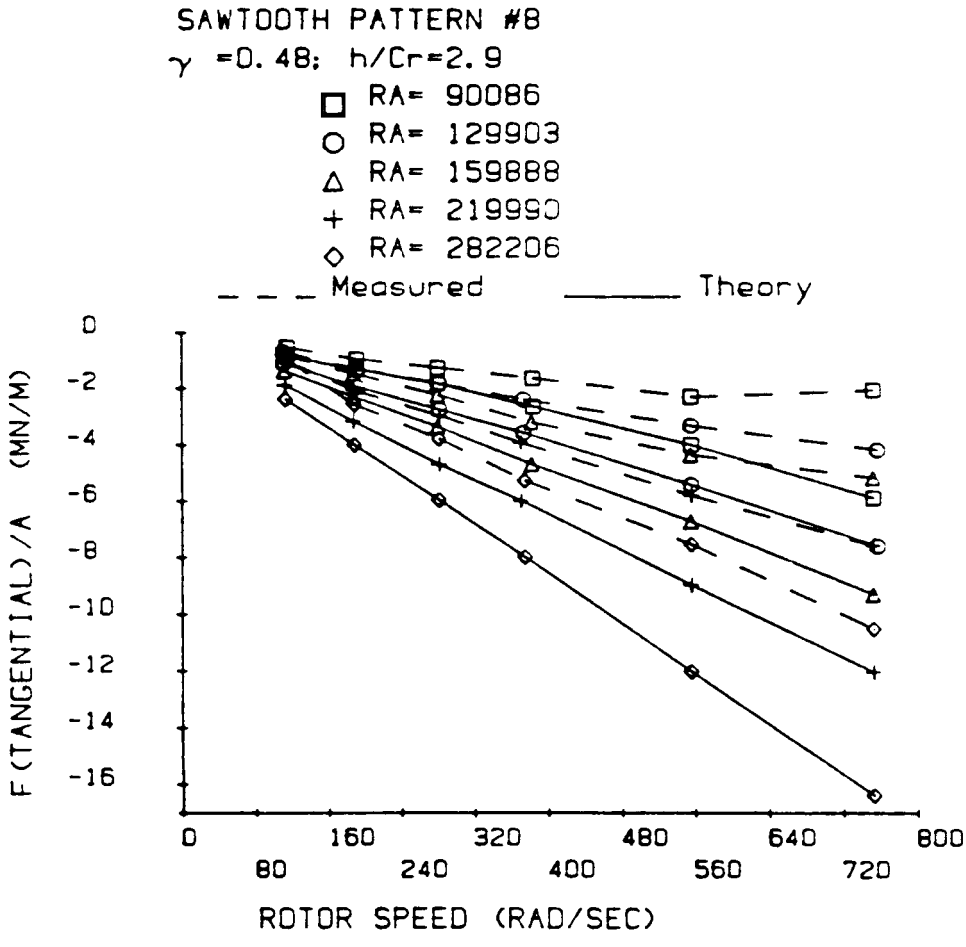

Fig. A2 Experimental and theoretical results for tangential force coefficients for stator 8

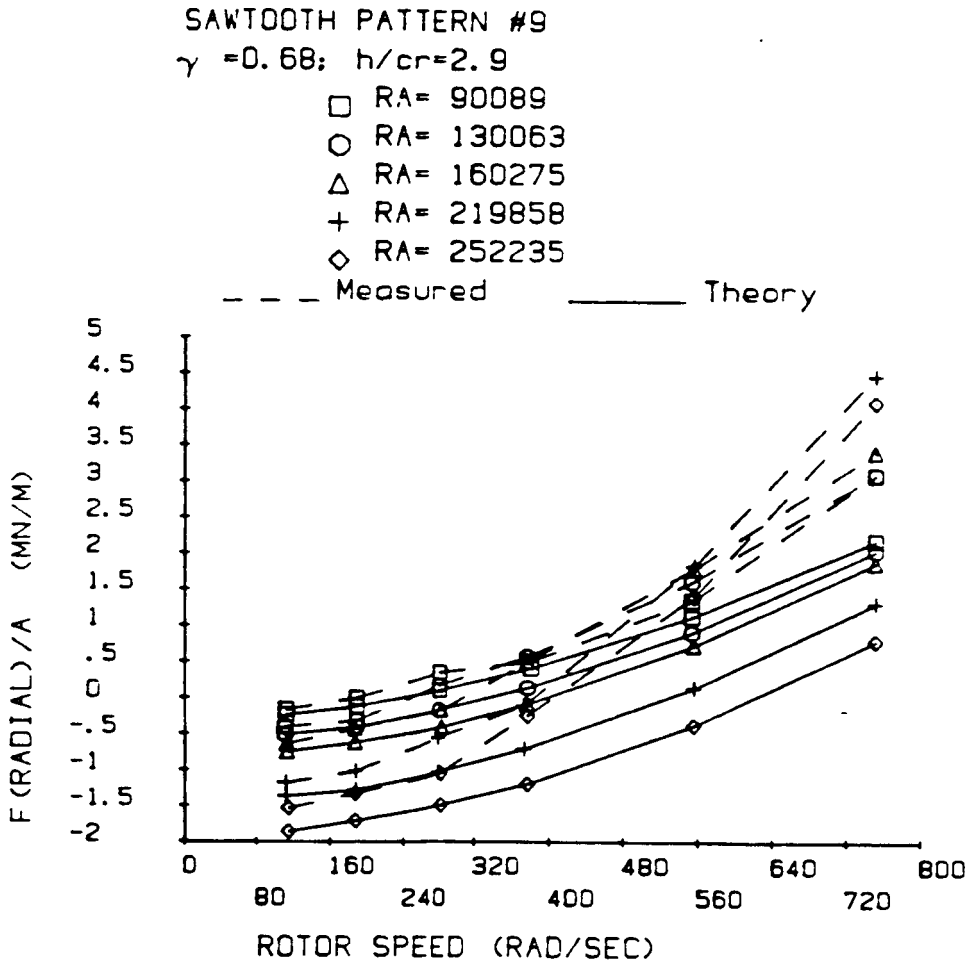

Fig. A3 Experimental and theoretical results for radial force coefficients for stator 9

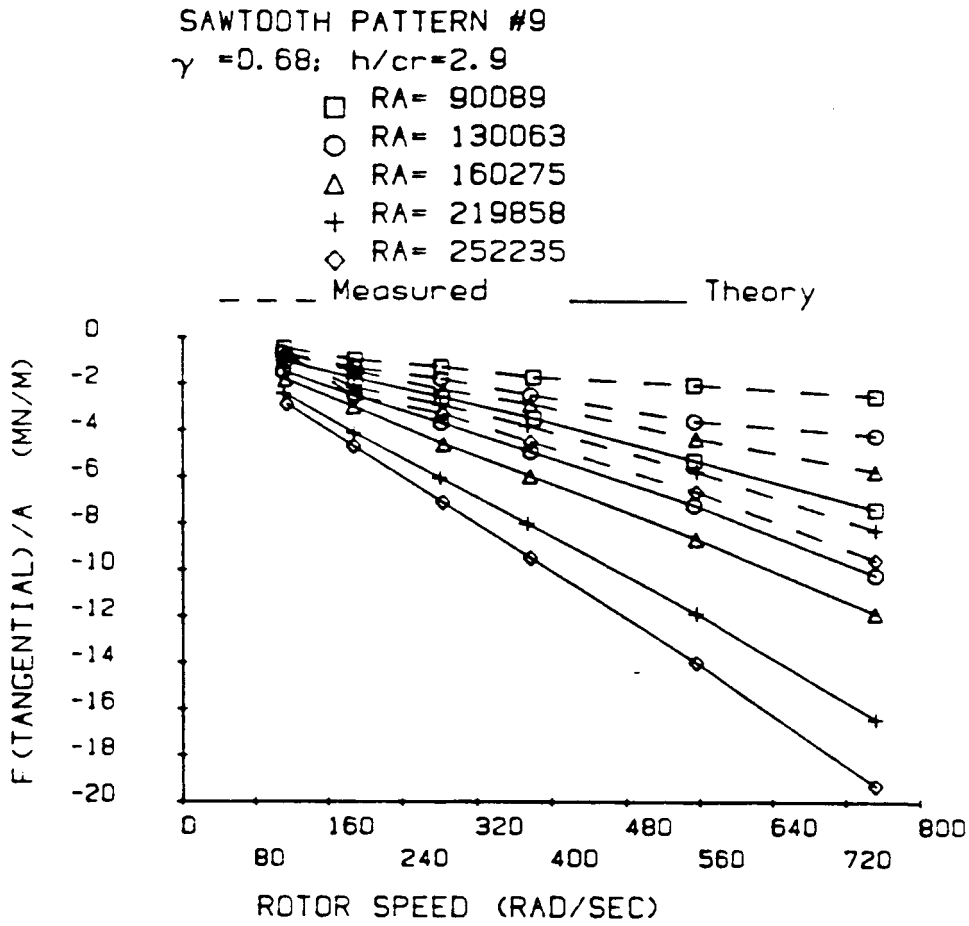

Fig. A4 Experimental and theoretical results for tangential force coefficients for stator 9

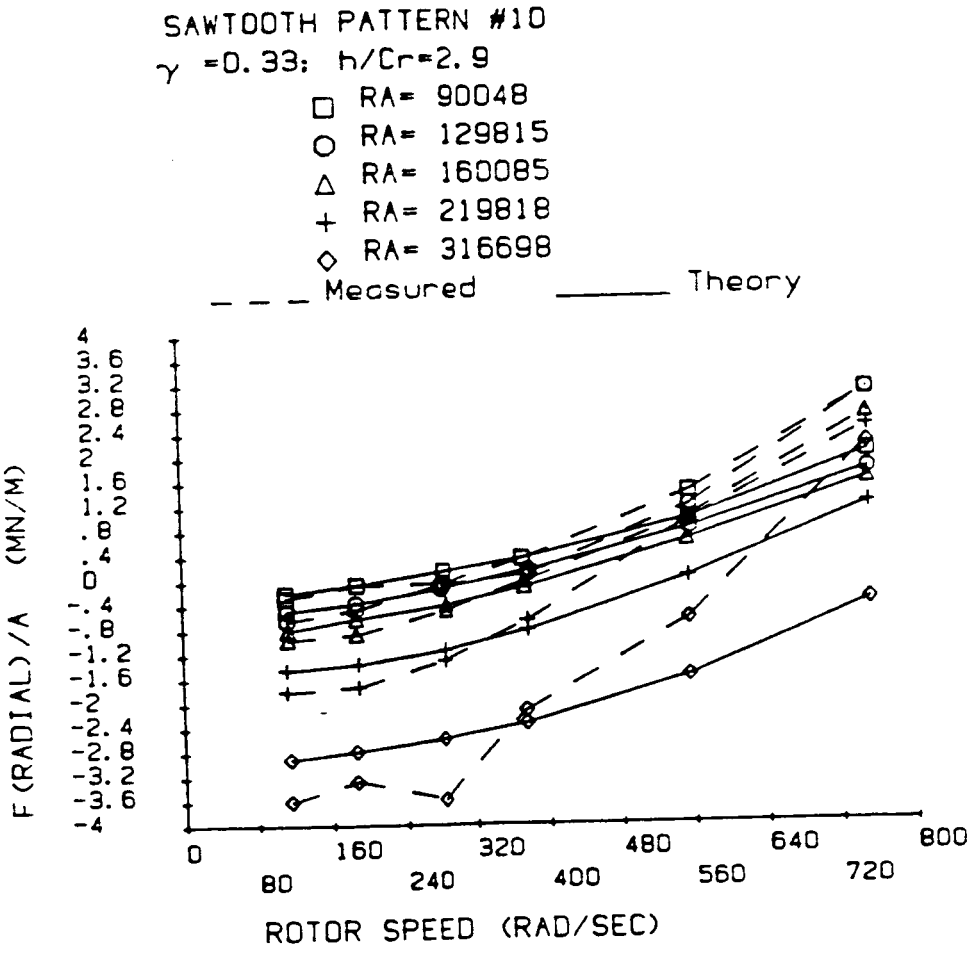

Fig. A5 Experimental and theoretical results for radial force coefficients for stator 10

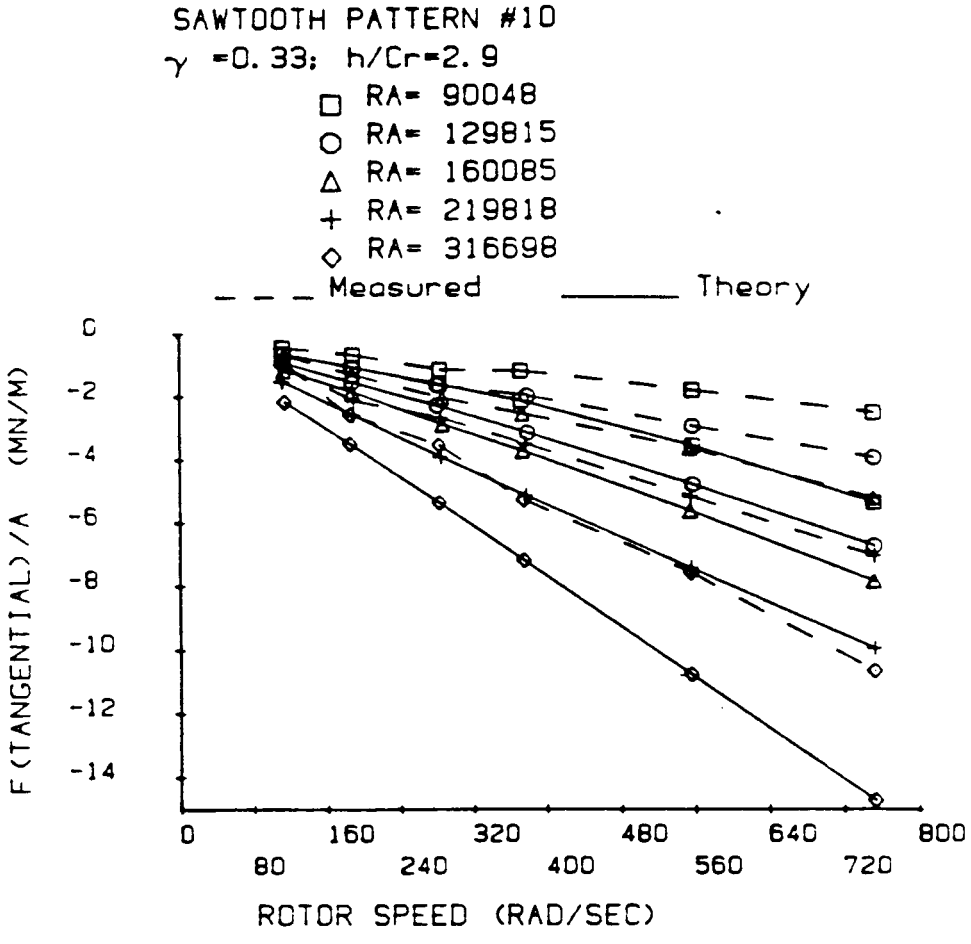

Fig. A6 Experimental and theoretical results for tangential force coefficients for stator 10

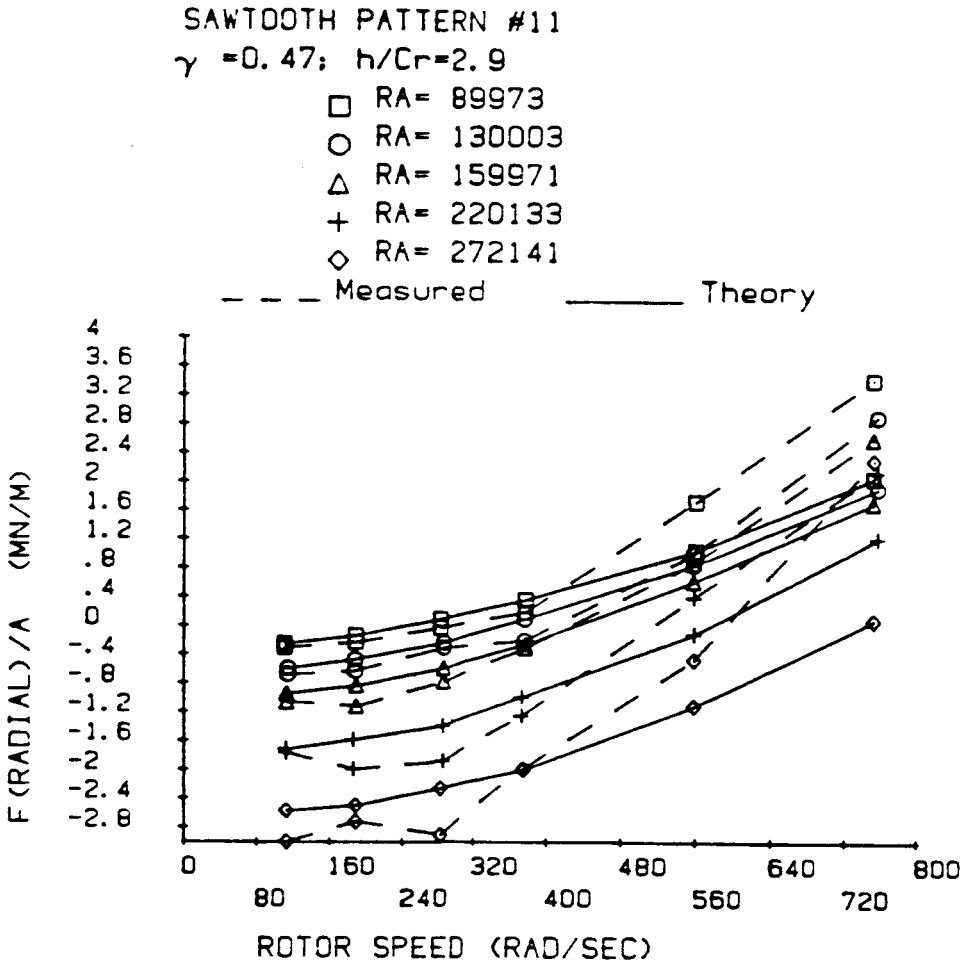

Fig. A7 Experimental and theoretical results for radial force coefficients for stator 11

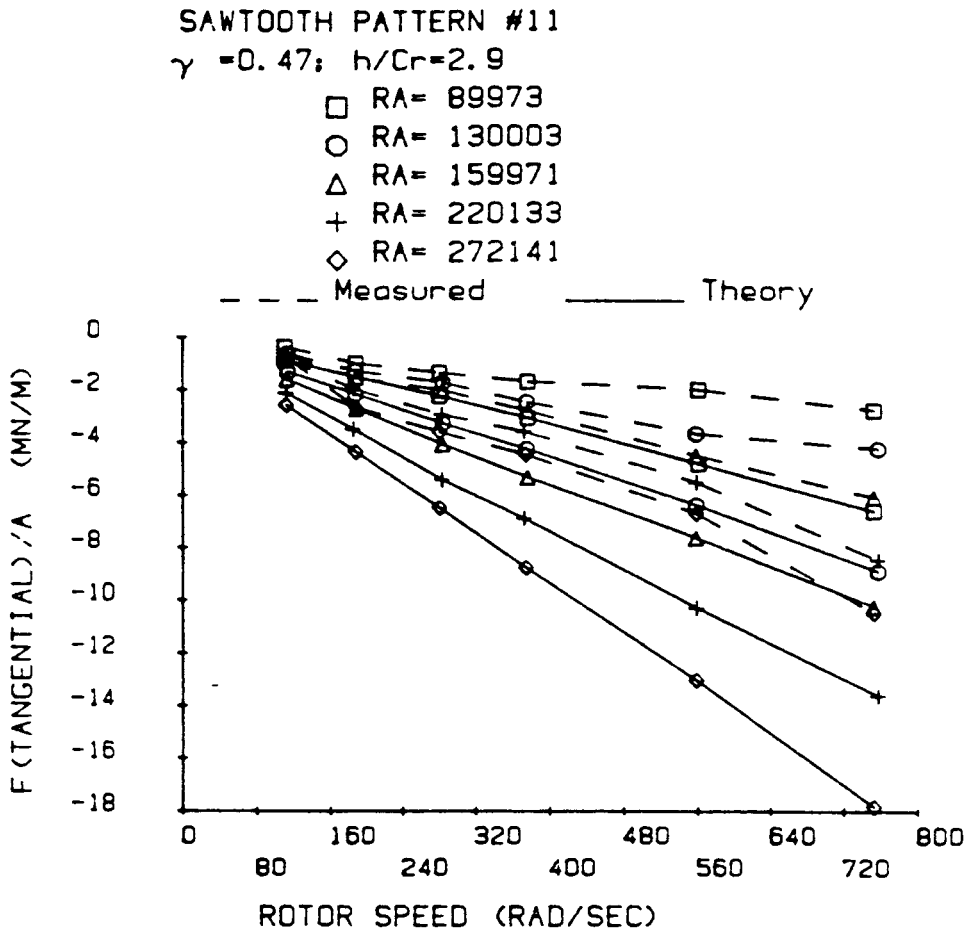

Fig. A8 Experimental and theoretical results for tangential force coefficients for stator 11